US 20240190789A1

(19) **United States**

(12) **Patent Application Publication**

(10) **Pub. No.: US 2024/0190789 A1**

(43) **Pub. Date: Jun. 13, 2024**

Zachariah et al.

(54) **MAGNESIUM VAPOR INDUCED SURFACE DISRUPTION OF METAL PARTICLES**

(71) Applicants: **The Regents of the University of California**, Oakland, CA (US); **University of Maryland**, College Park, MD (US)

(72) Inventors: **Michael R. Zachariah**, Riverside, CA (US); **Reza Abbaschian**, Riverside, CA (US); **Pankaj Ghildiyal**, College Park, MD (US); **Steven Herrera**, Riverside, CA (US)

(21) Appl. No.: **18/534,467**

(22) Filed: **Dec. 8, 2023**

Related U.S. Application Data

(60) Provisional application No. 63/386,561, filed on Dec. 8, 2022.

Publication Classification

(51) **Int. Cl.**

C06B 33/00 (2006.01)

C06B 21/00 (2006.01)

(52) **U.S. Cl.**

CPC ***C06B 33/00*** (2013.01); ***C06B 21/0091*** (2013.01)

(57) **ABSTRACT**

Compositions comprising magnesium nanoparticles, a nanoscale metal or metalloid, and an oxidizer and methods of fabrication the compositions are described. One example use of such compositions is in high energy fuel applications. One example method includes fabricating a composite by adding magnesium nanoparticles to a composition of a nanoscale metal or metalloid and an oxidant. Examples of the composition resulting from the described processes provides shorter burn times and a multi-fold increase in reactivity compared to the corresponding composition comprising the same amount of nanoscale metal or metalloid and oxidizer but without the magnesium nanoparticles.

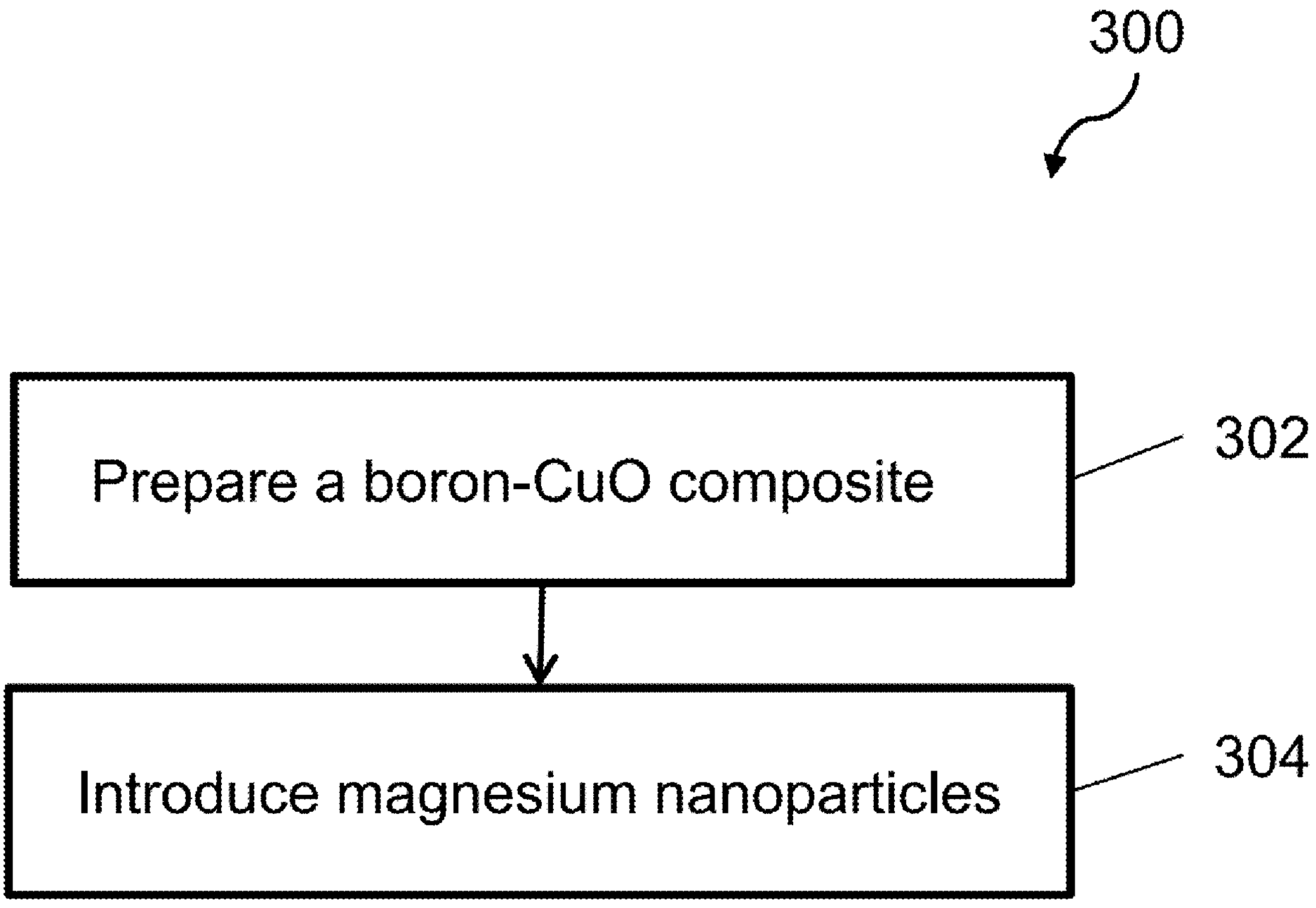

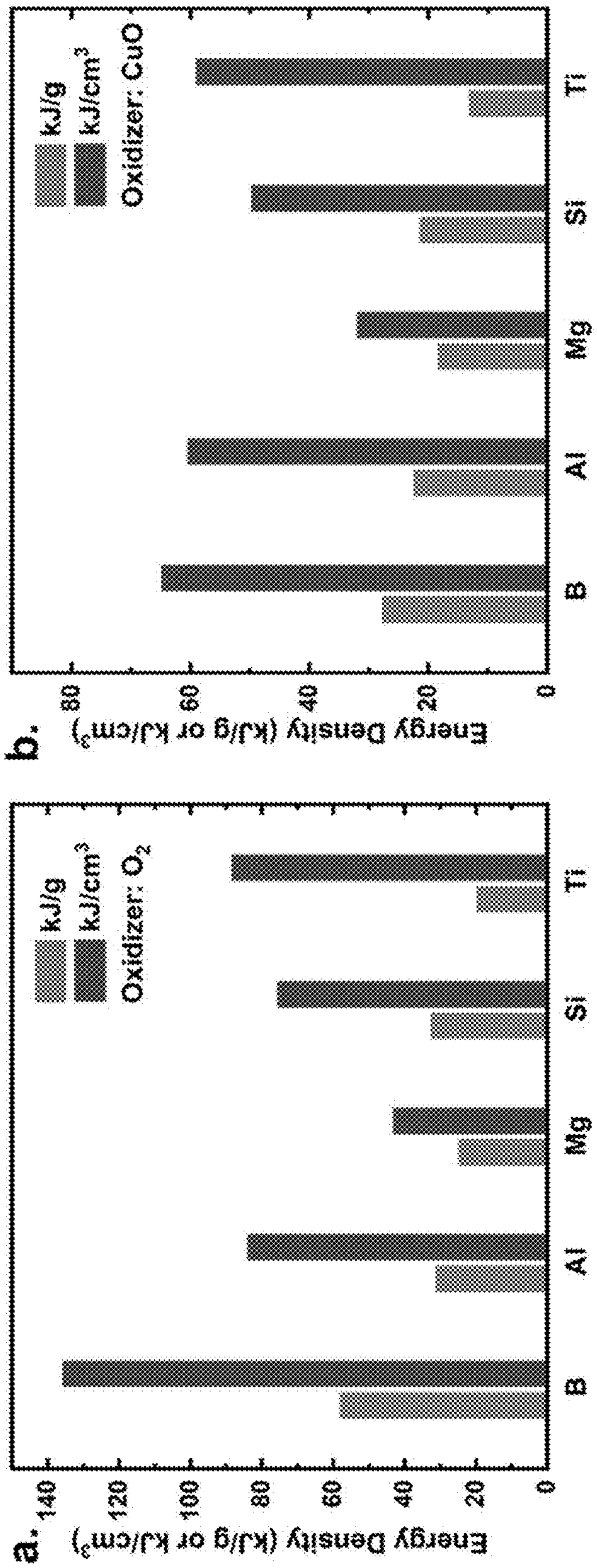
kJ/g
kJ/cm3
Oxidizer: CuO
Ti
Si
Mg
Al
B
Energy Density (kJ/g or kJ/cm3)
0
20
40
60
80
b.
kJ/g
kJ/cm3
Oxidizer: O2
Ti
Si
Mg
Al
B
Energy Density (kJ/g or kJ/cm3)
0
20
40
60
80
100
120
140
a.

FIG. 1A

FIG. 1B

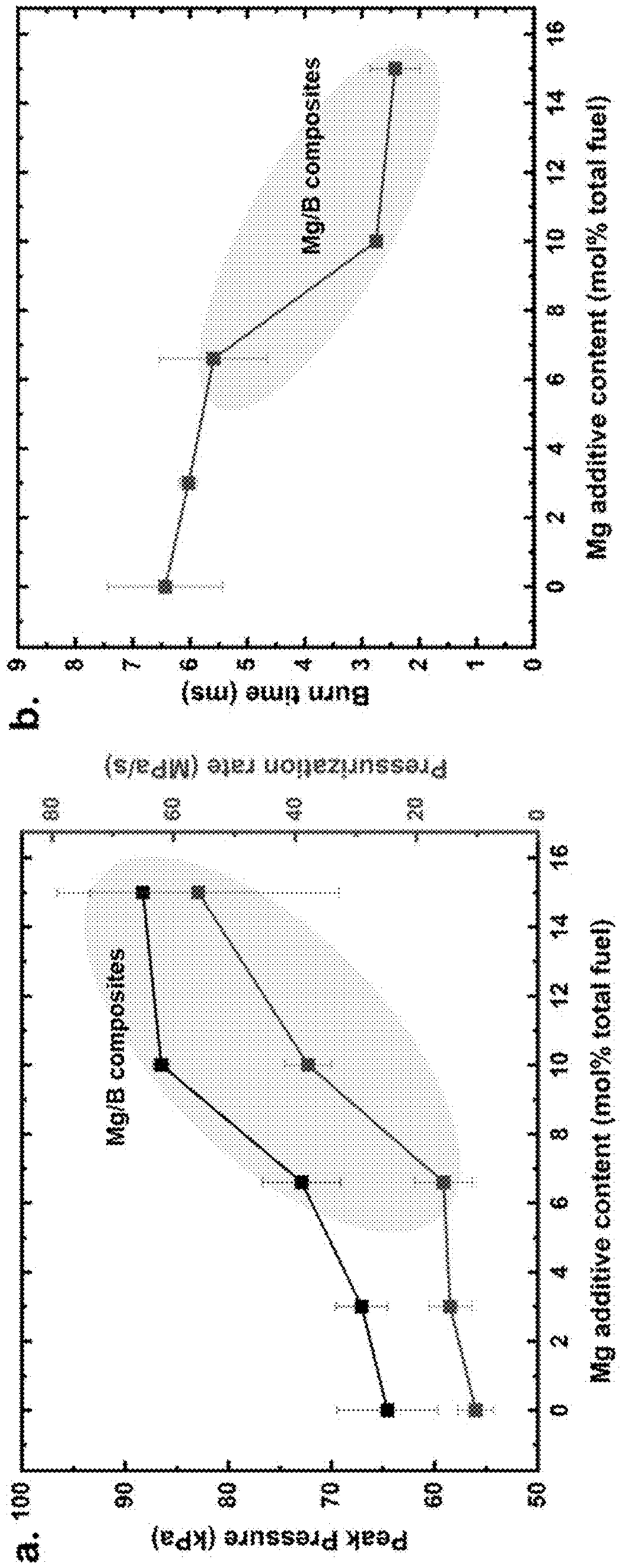
b.
Burn time (ms)
0
1
2
3
4
5
6
7
8
9
Mg/B composites
Mg additive content (mol% total fuel)
0
2
4
6
8
10
12
14
16
a.
Peak Pressure (kPa)
50
60
70
80
90
100
Mg/B composites
Mg additive content (mol% total fuel)
0
2
4
6
8
10
12
14
16
Pressurization rate (MPa/s)
0
20
40
60
80

FIG. 2B

FIG. 2A

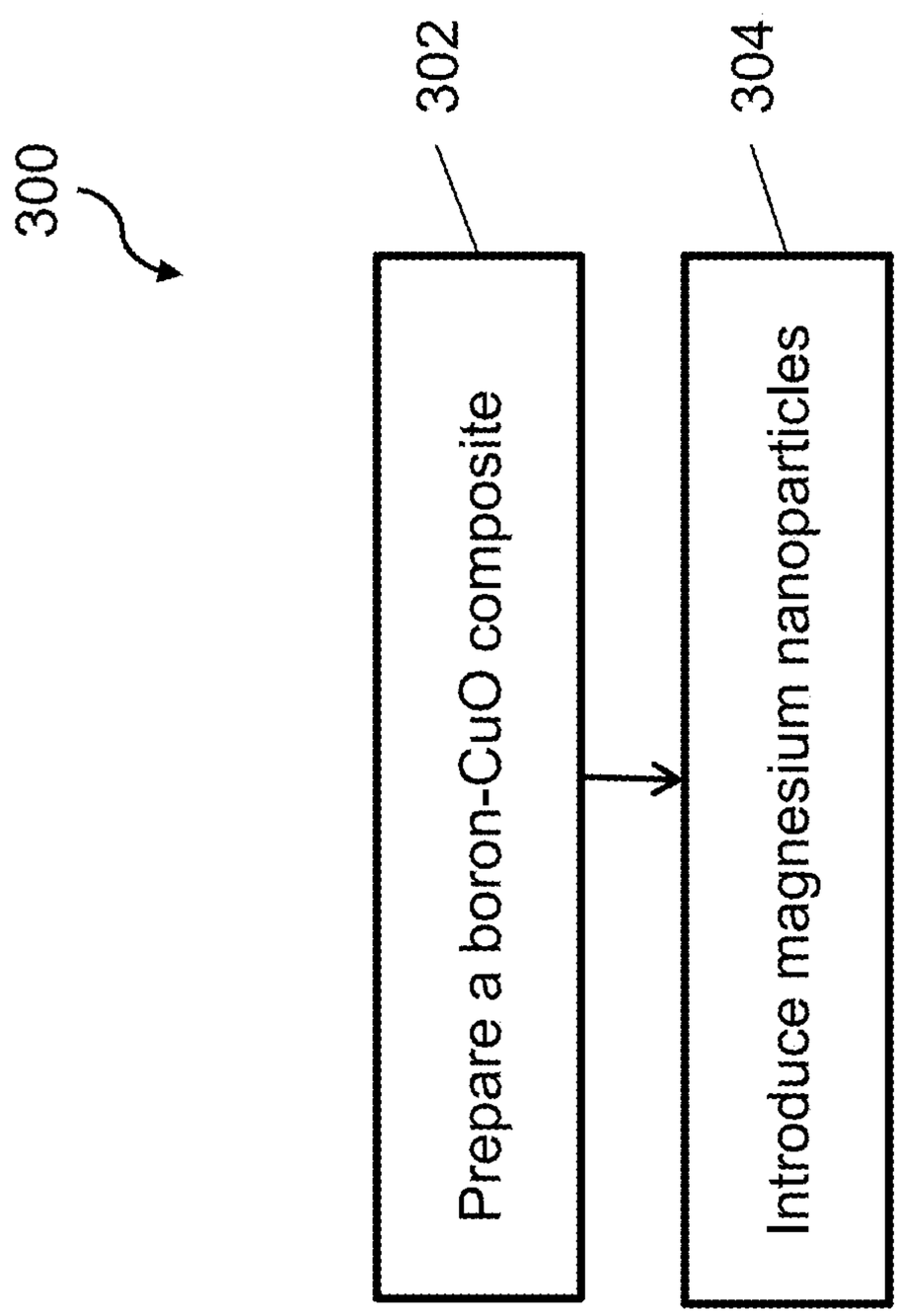
300
302
Prepare a boron-CuO composite
304
Introduce magnesium nanoparticles

FIG. 3

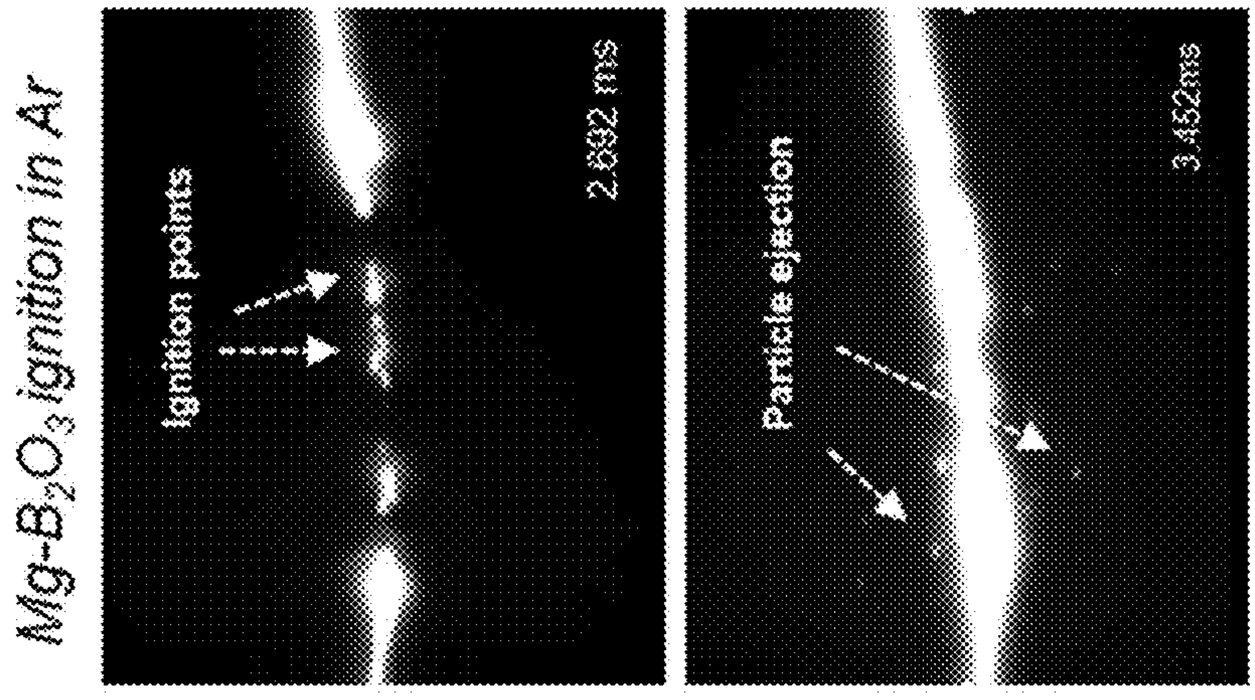
Mg-B2O3 ignition in Ar
Ignition points
2.692 ms
Particle ejection
3.452ms

FIG. 4B

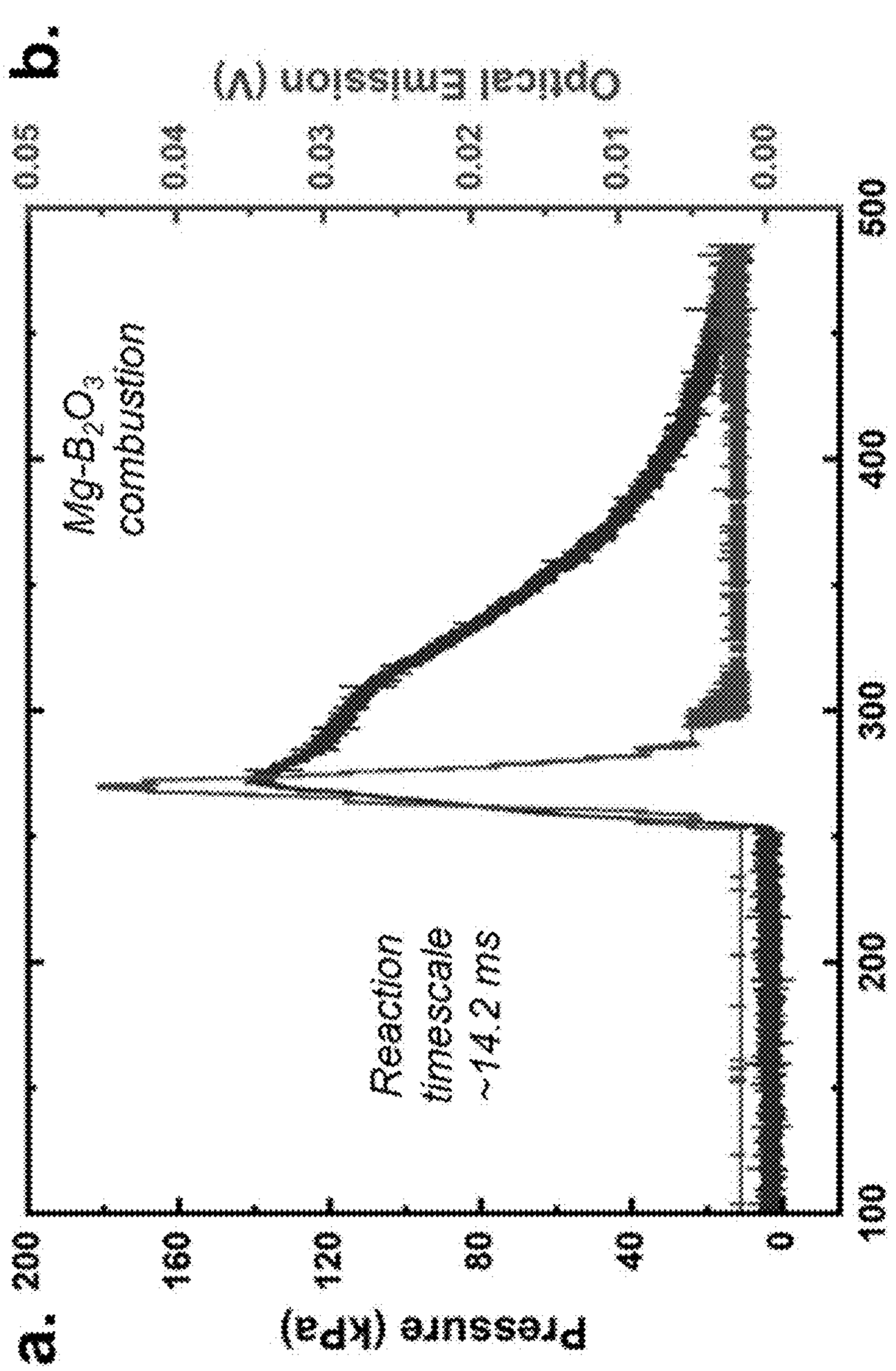
b.
Optical Emission (V)
0.05
0.04
0.03
0.02
0.01
0.00
Mg-B2O3 combustion
Reaction timescale ~14.2 ms
Time (ms)
500
400
300
200
100
a.
Pressure (kPa)
200
160
120
80
40
0

FIG. 4A

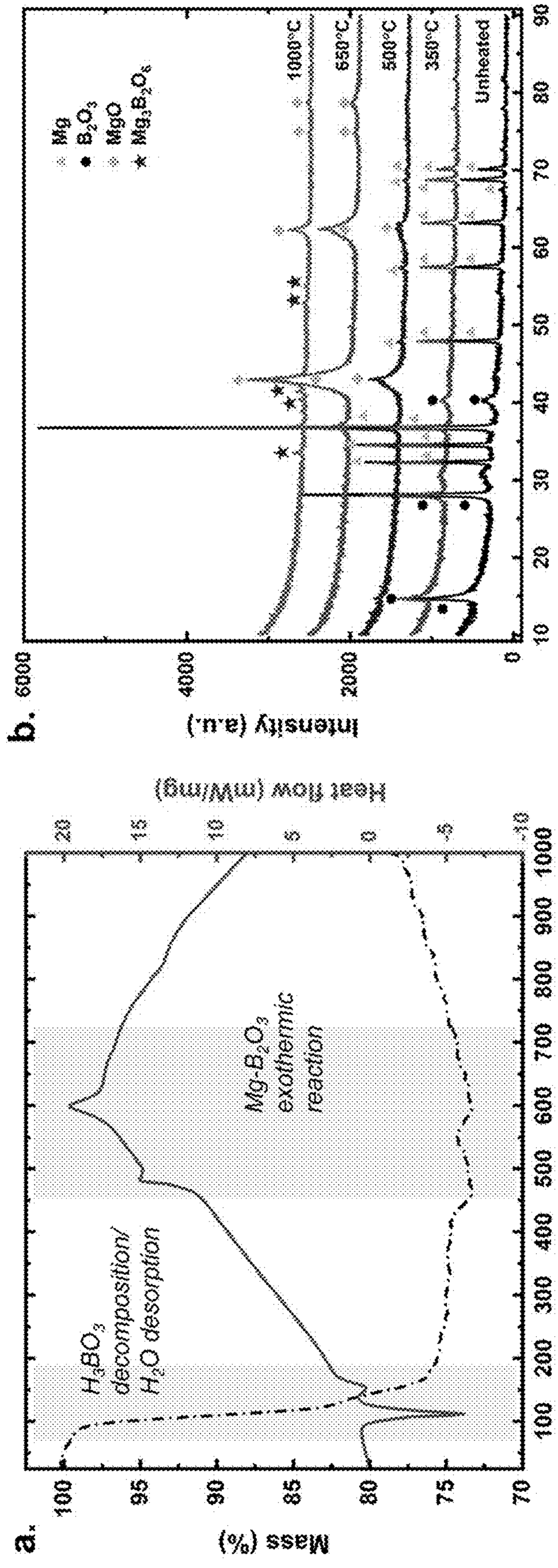
Mg
B_2O_3
MgO
$Mg_3B_2O_6$
1000°C
650°C
500°C
350°C
Unheated
Angle, 2θ (°)
Intensity (a.u.)
b.
Heat flow (mW/mg)
H_3BO_3 decomposition/ H_2O desorption
Mg-B_2O_3 exothermic reaction
Mass (%)
Temperature (°C)
a.

FIG. 5B

FIG. 5A

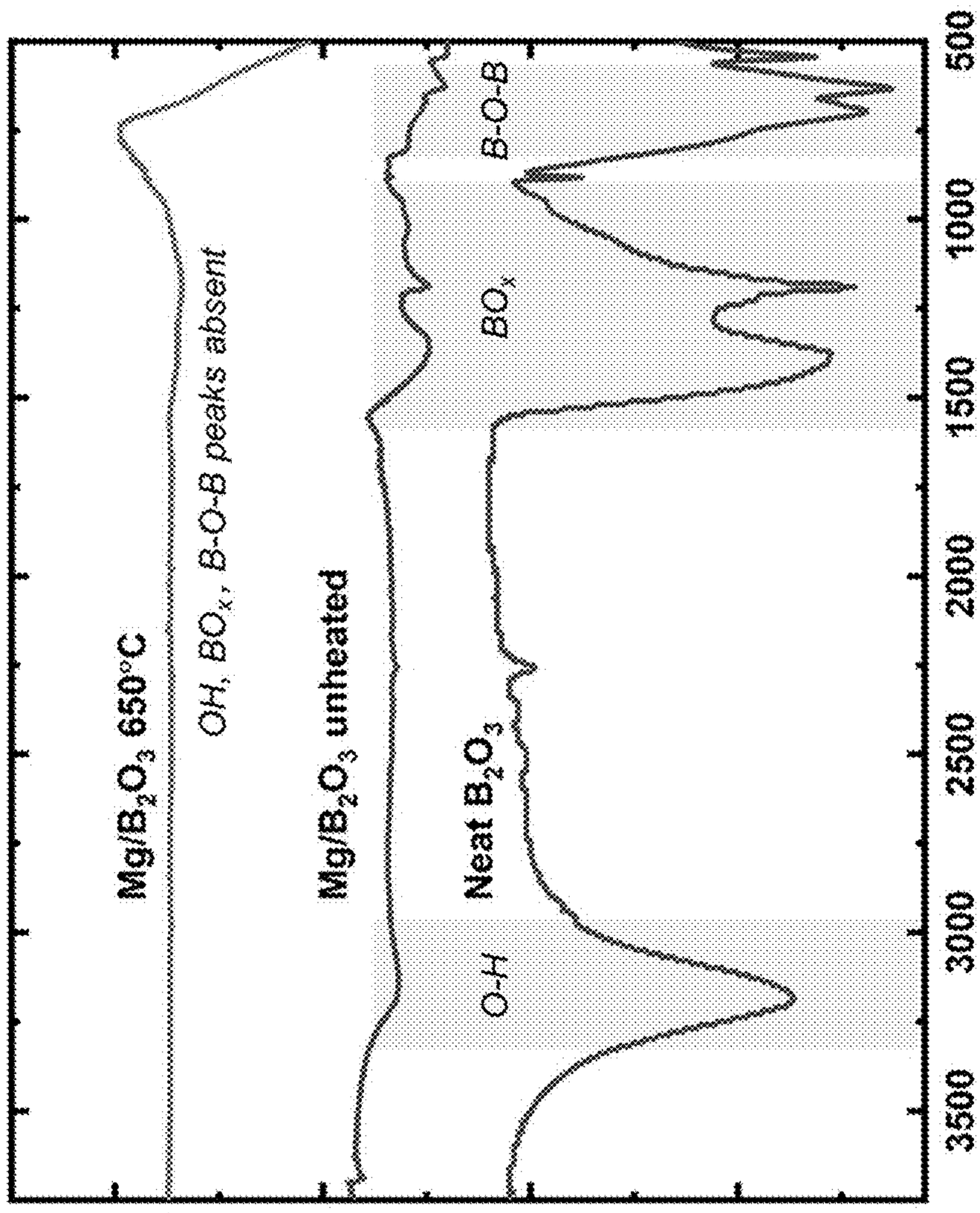
Mg/B2O3 650°C
OH, BOx, B-O-B peaks absent
Mg/B2O3 unheated
Neat B2O3
O-H
B-O-B
BOx
Transmittance (a.u.)
Wavenumber (cm-1)
3500
3000
2500
2000
1500
1000
500

FIG. 6

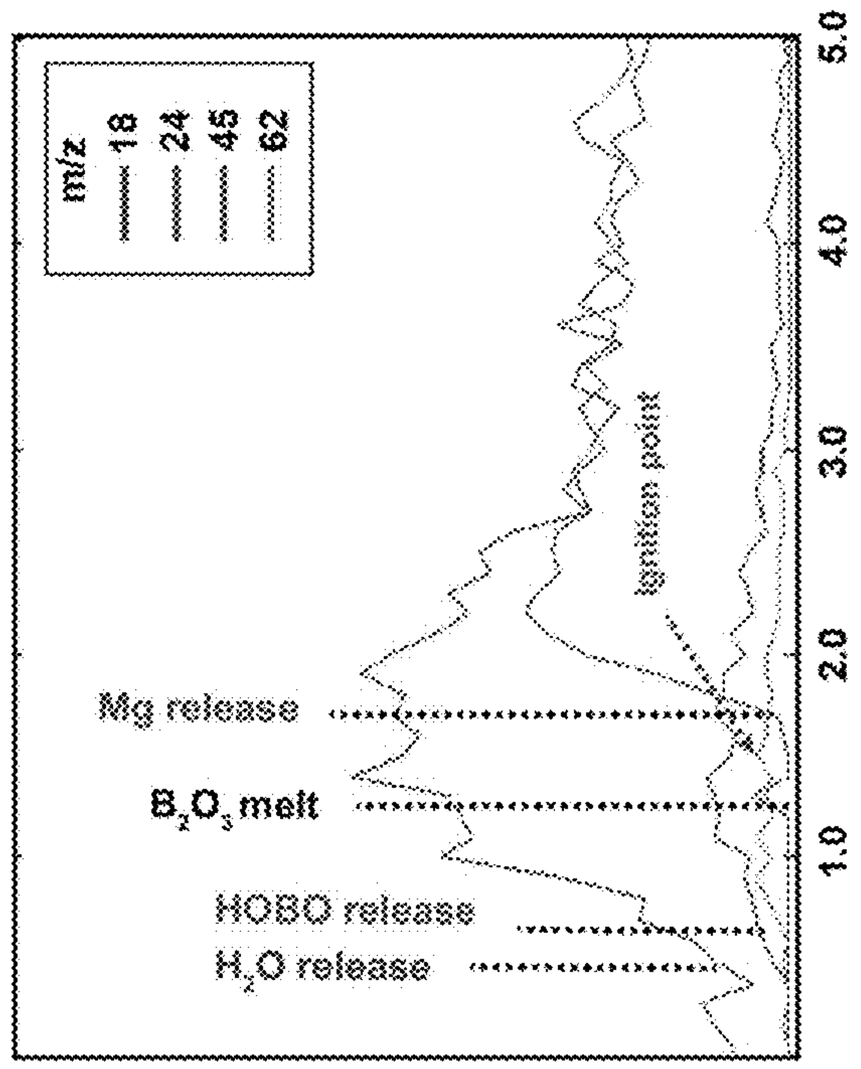
m/z
18
24
45
62
Mg release
B_2O_3 melt
HOBO release
H_2O release
Ignition point
Time (ms)
5.0
4.0
3.0
2.0
1.0
Signal Intensity (a.u.)

FIG. 7B

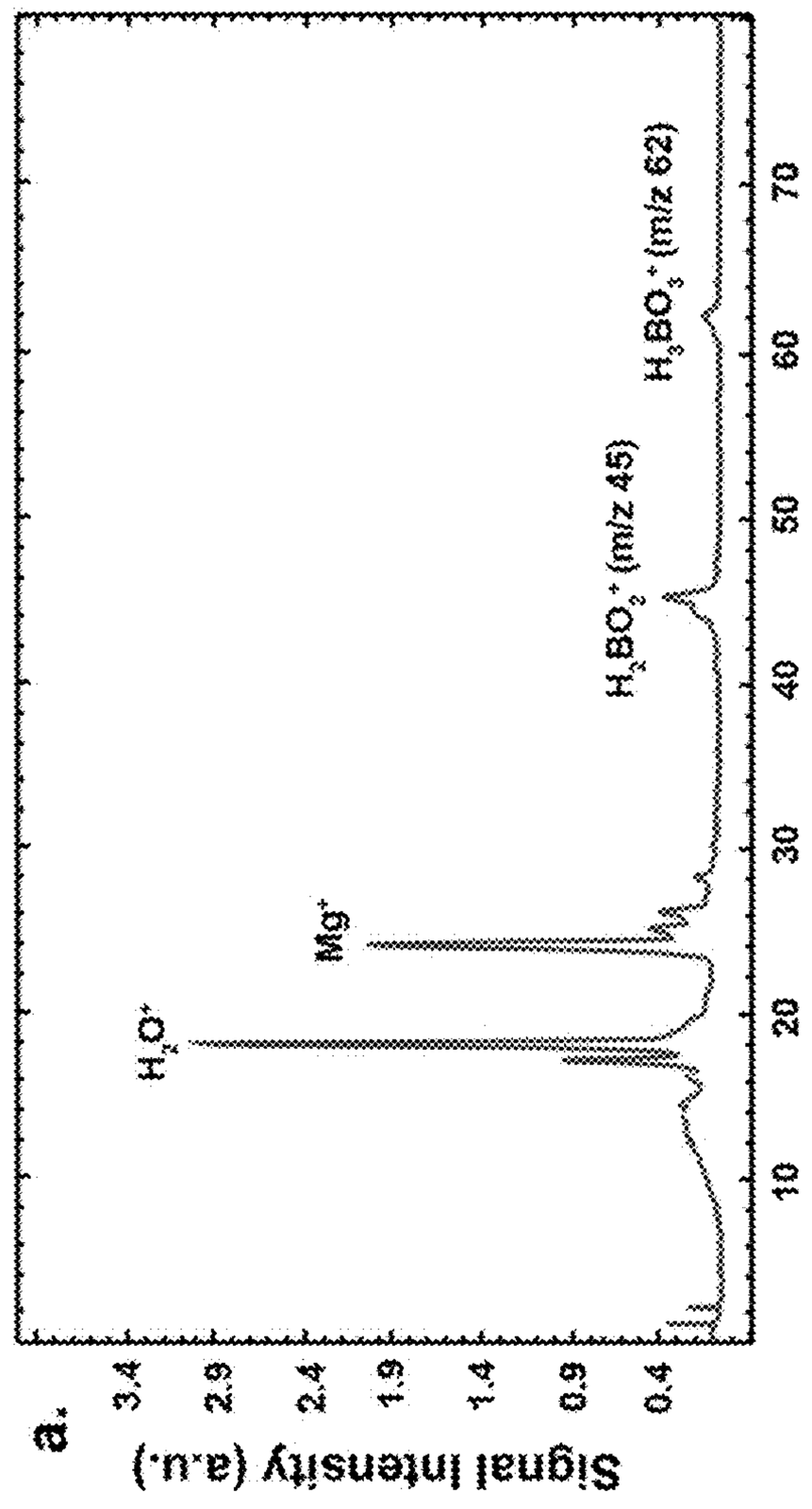
H_2O^+
Mg^+
$H_2BO_2^+$ (m/z 45)
$H_3BO_3^+$ (m/z 62)
m/z
10
20
30
40
50
60
70
Signal Intensity (a.u.)
0.4
0.9
1.4
1.9
2.4
2.9
3.4

FIG. 7A

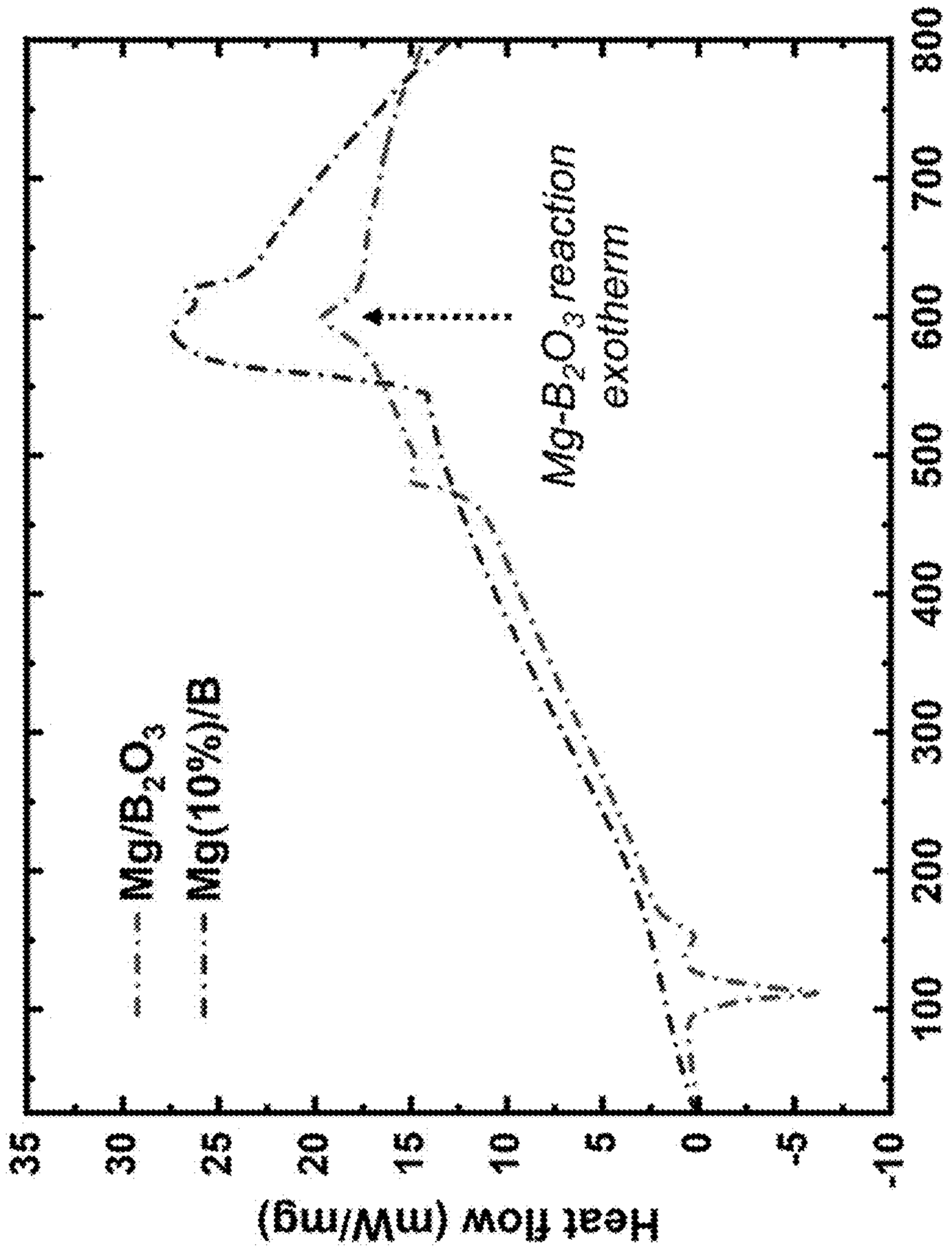
Mg/B2O3
Mg(10%)/B
Mg-B2O3 reaction
exotherm
Heat flow (mW/mg)
Temperature (°C)
35
30
25
20
15
10
5
0
5
10
100
200
300
400
500
600
700
800

FIG. 8

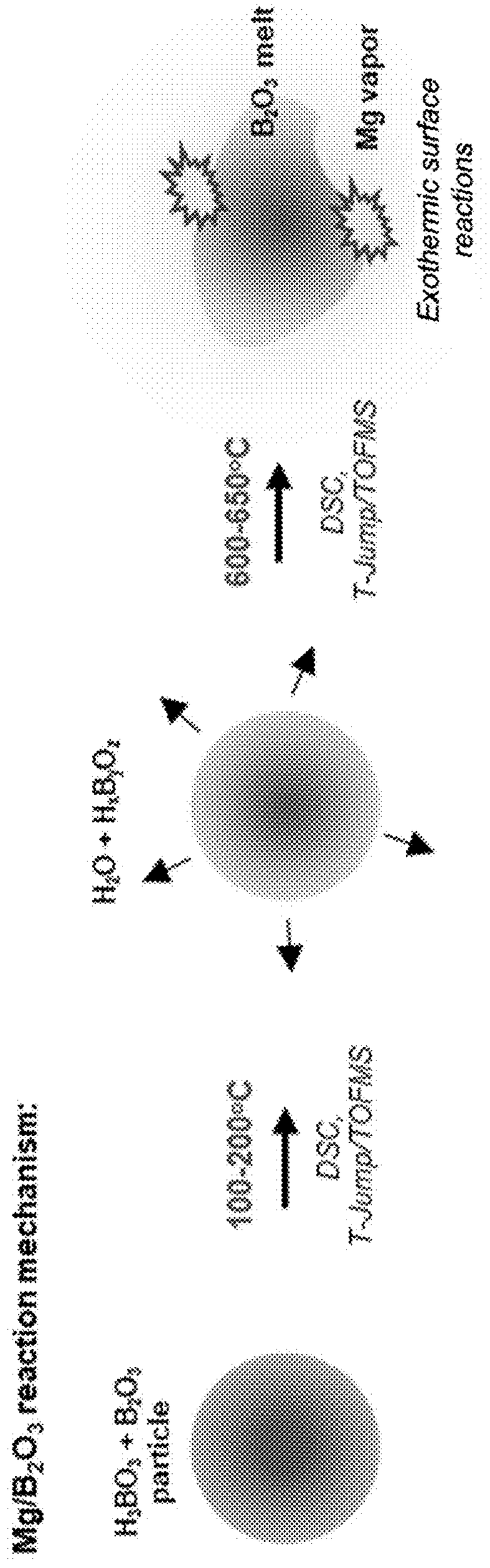
Mg/B2O3 reaction mechanism:
H3BO3 + B2O3 particle
100-200°C
DSC, T-Jump/TOFMS
H2O + HxBOy
600-650°C
DSC, T-Jump/TOFMS
B2O3 melt
Mg vapor
Exothermic surface reactions

FIG. 9A

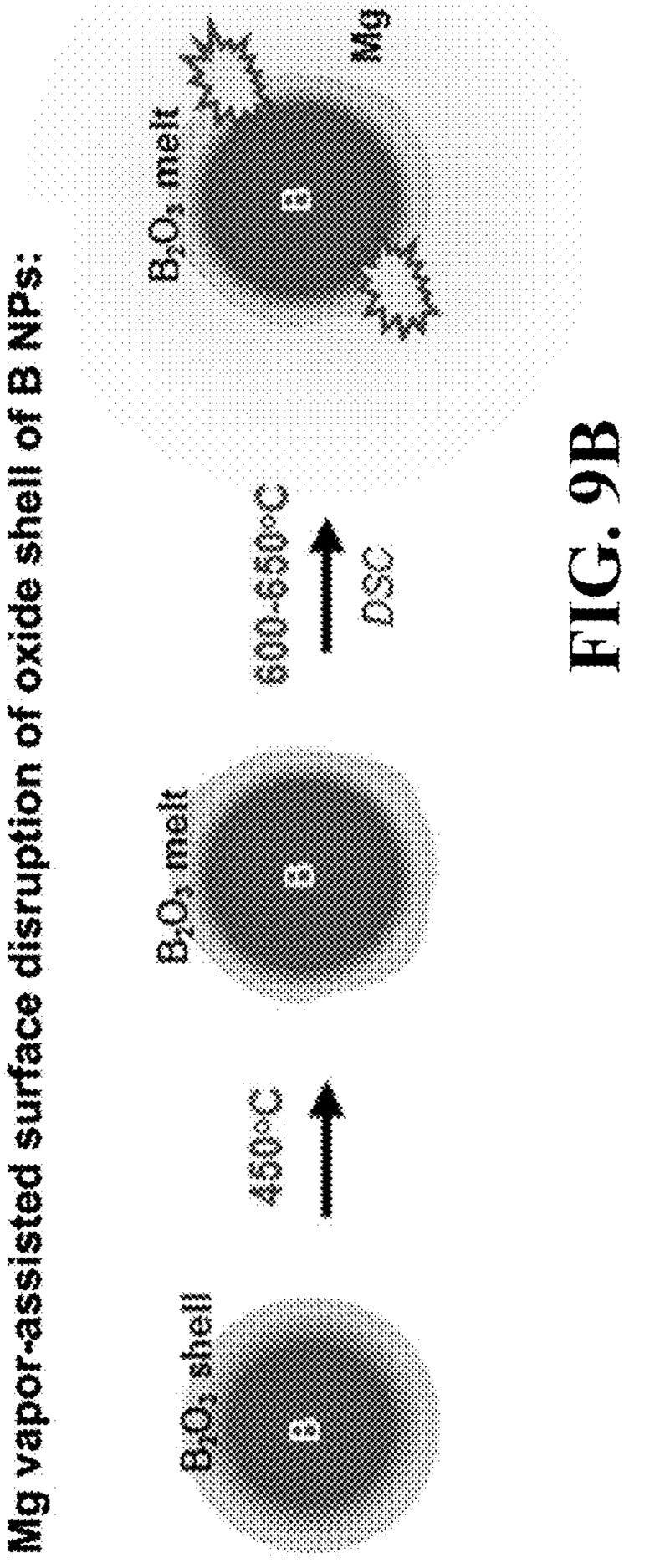
Mg vapor-assisted surface disruption of oxide shell of B NPs:
B2O3 shell
450°C
DSC
B2O3 melt
Mg vapor
Exothermic surface reactions

FIG. 9B

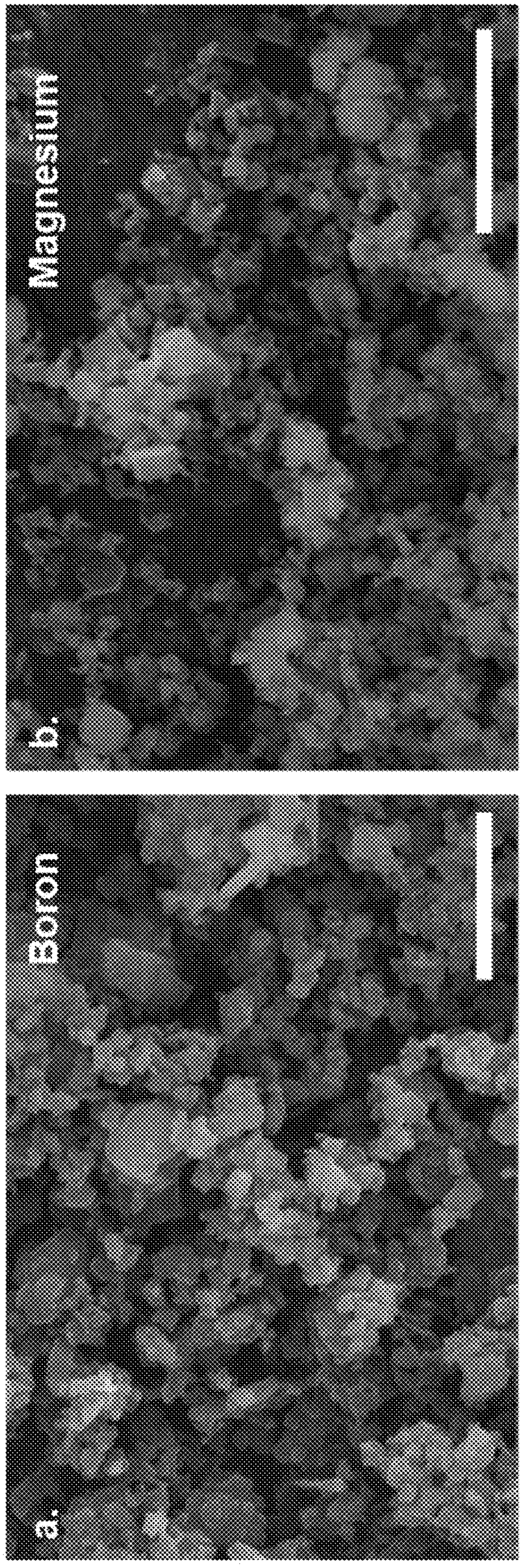

FIG. 10A

FIG. 10B

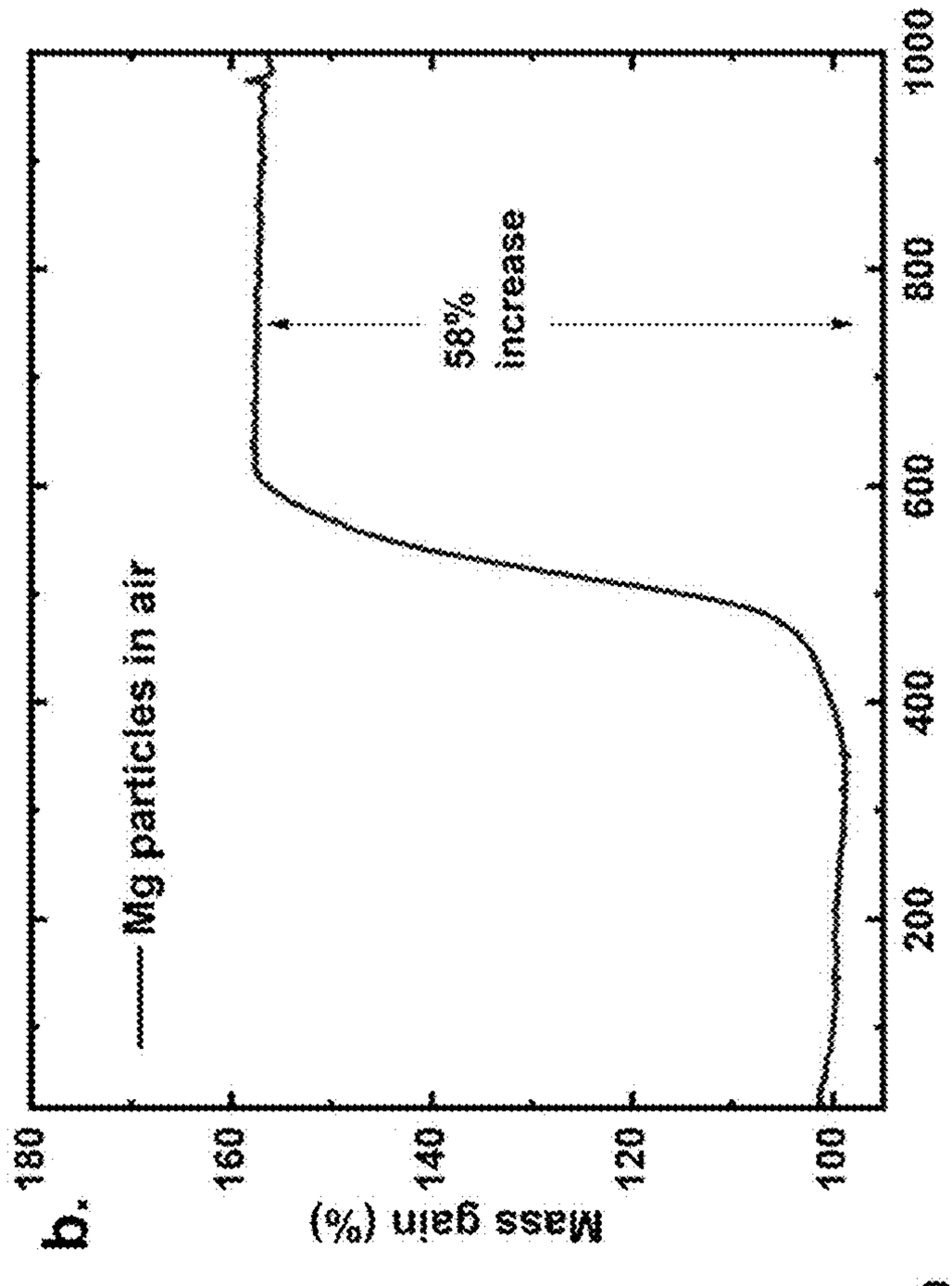

FIG. 11B

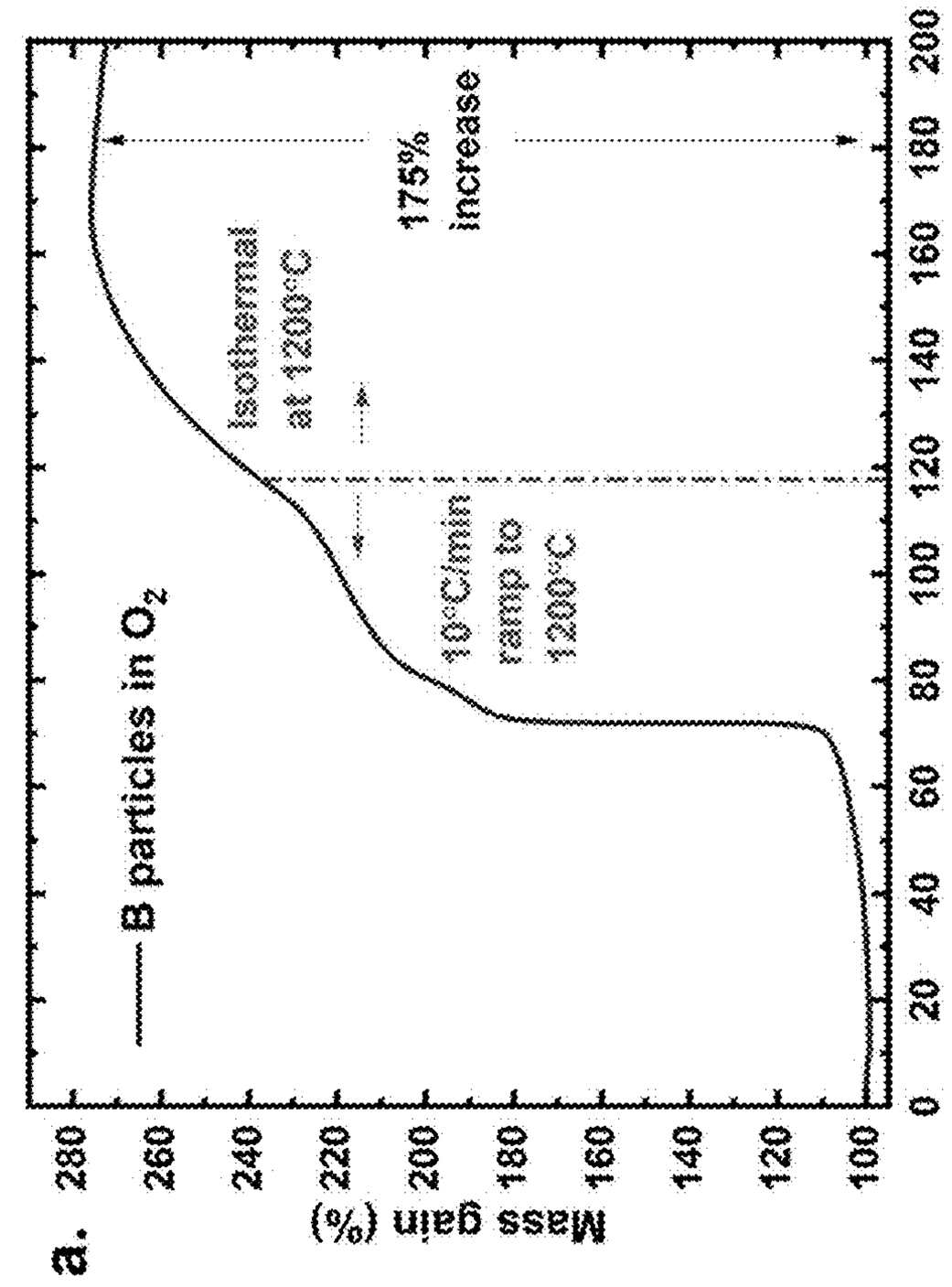

FIG. 11A

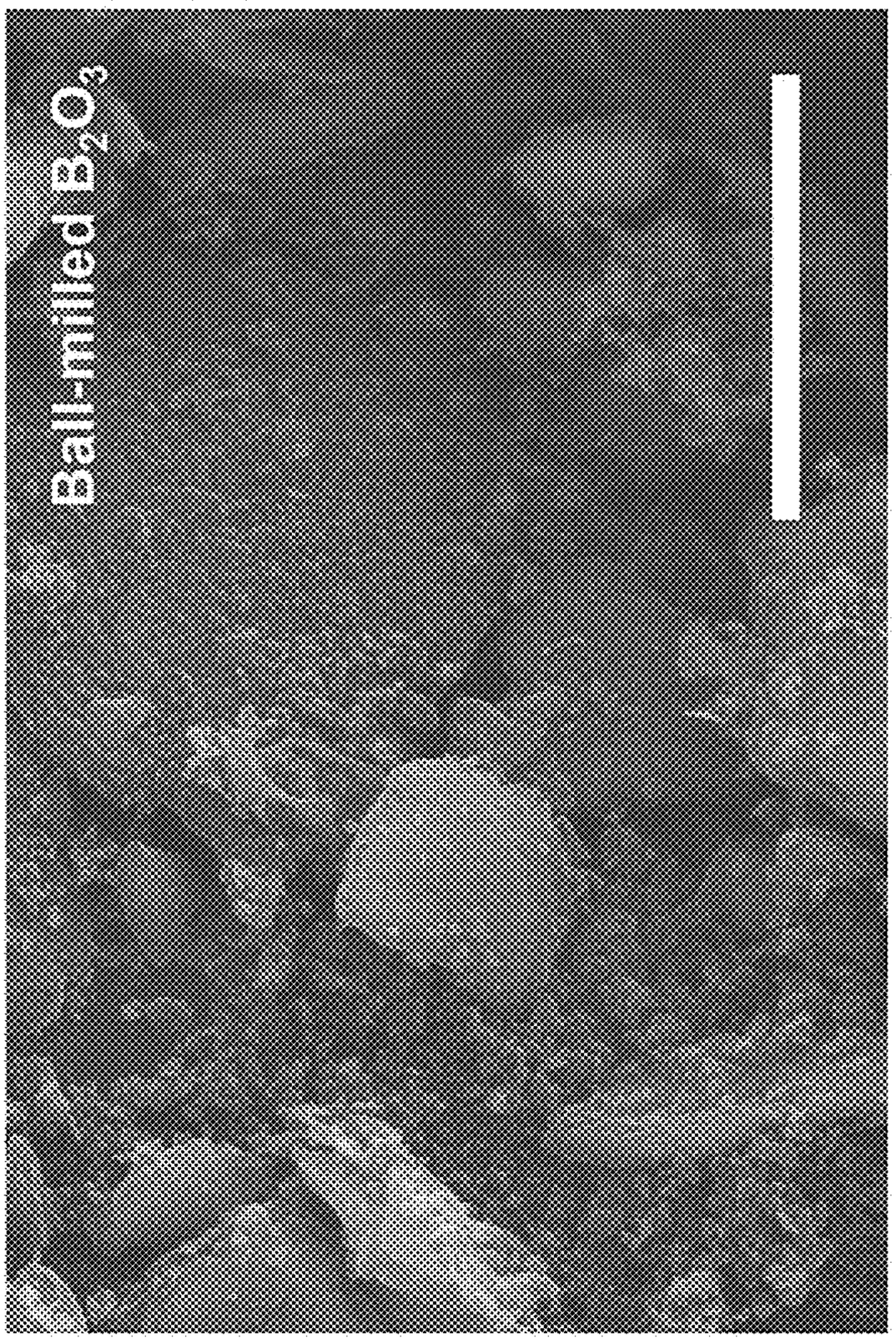

FIG. 12

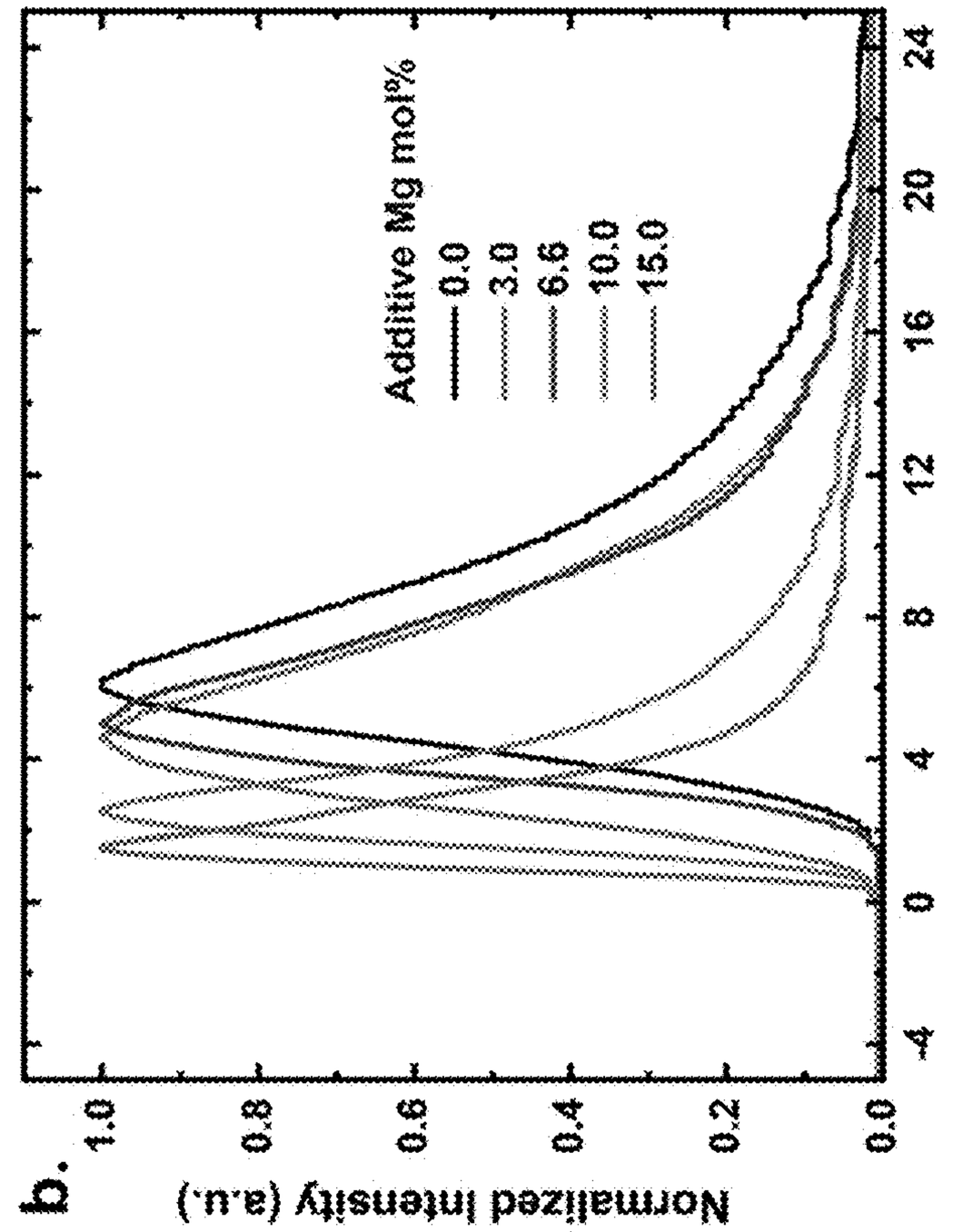

FIG. 13B

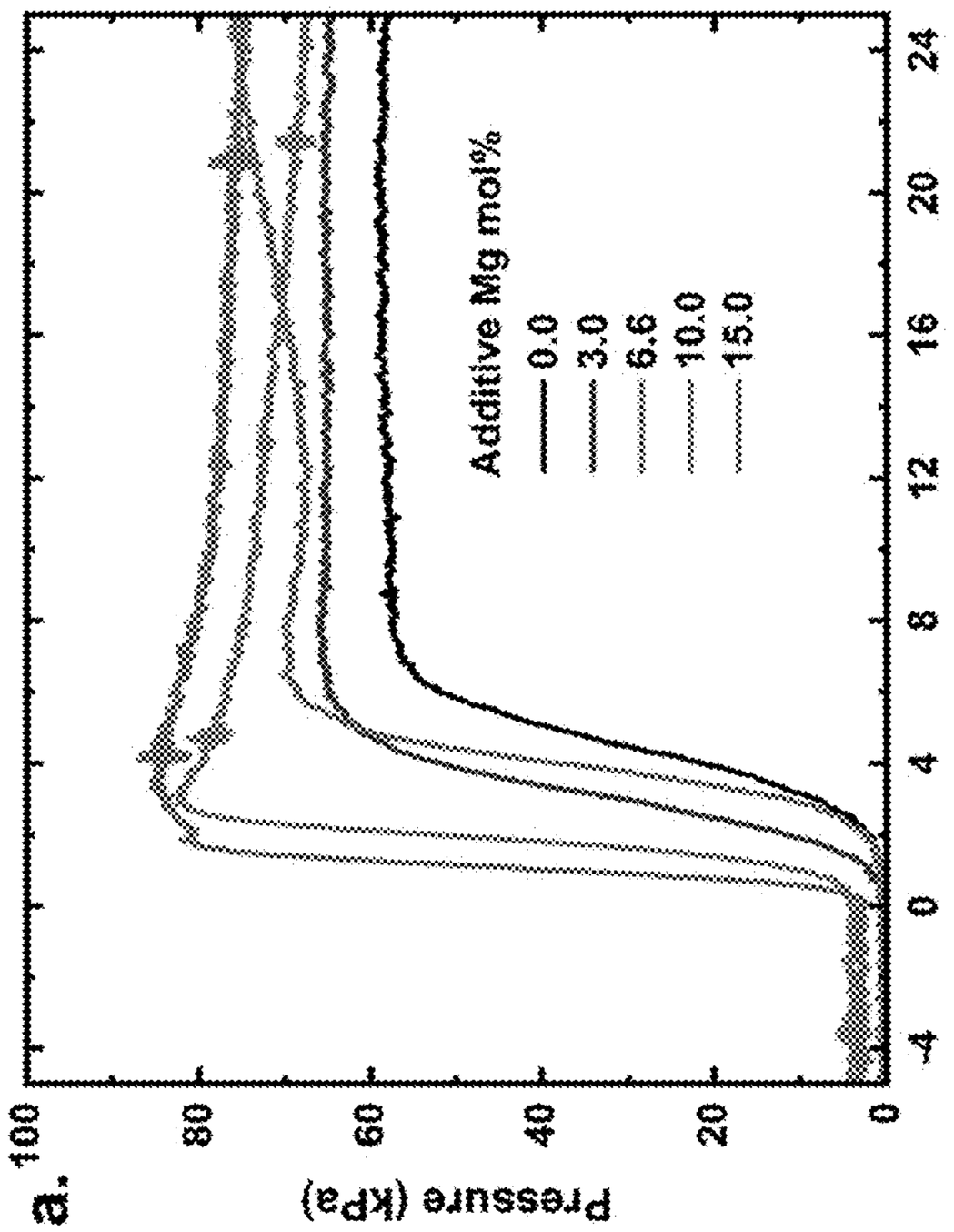

FIG. 13A

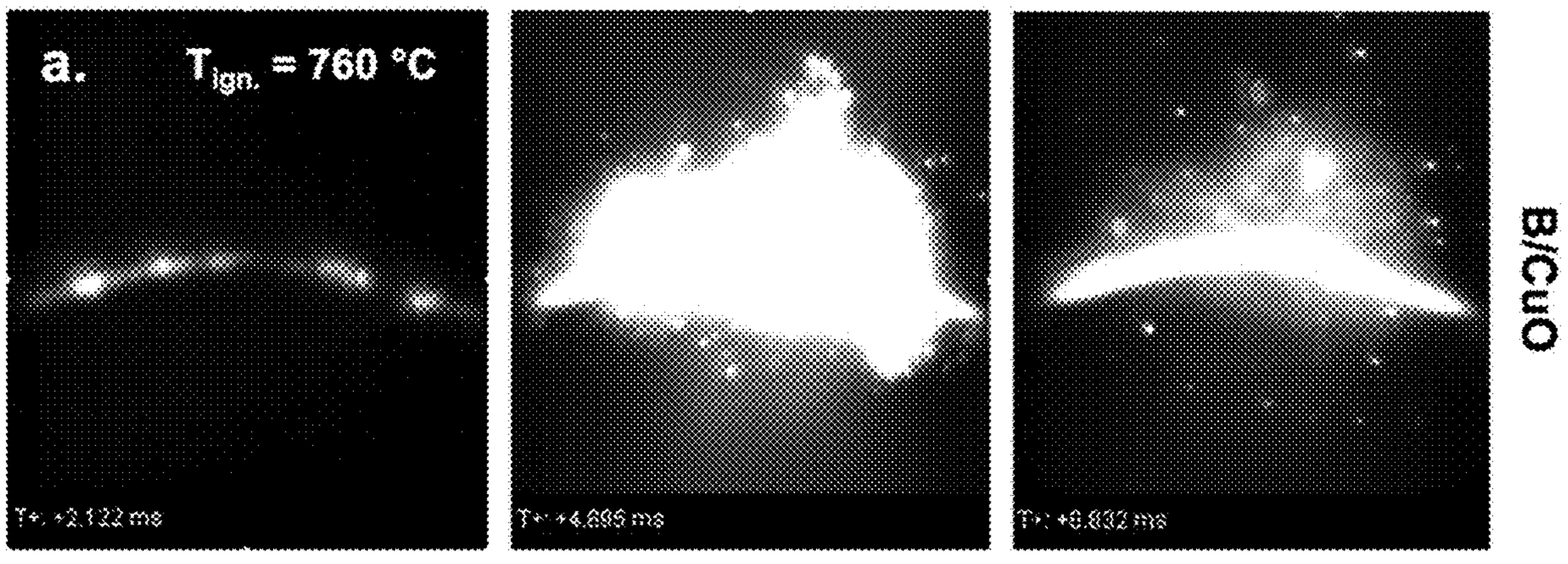

FIG. 14A

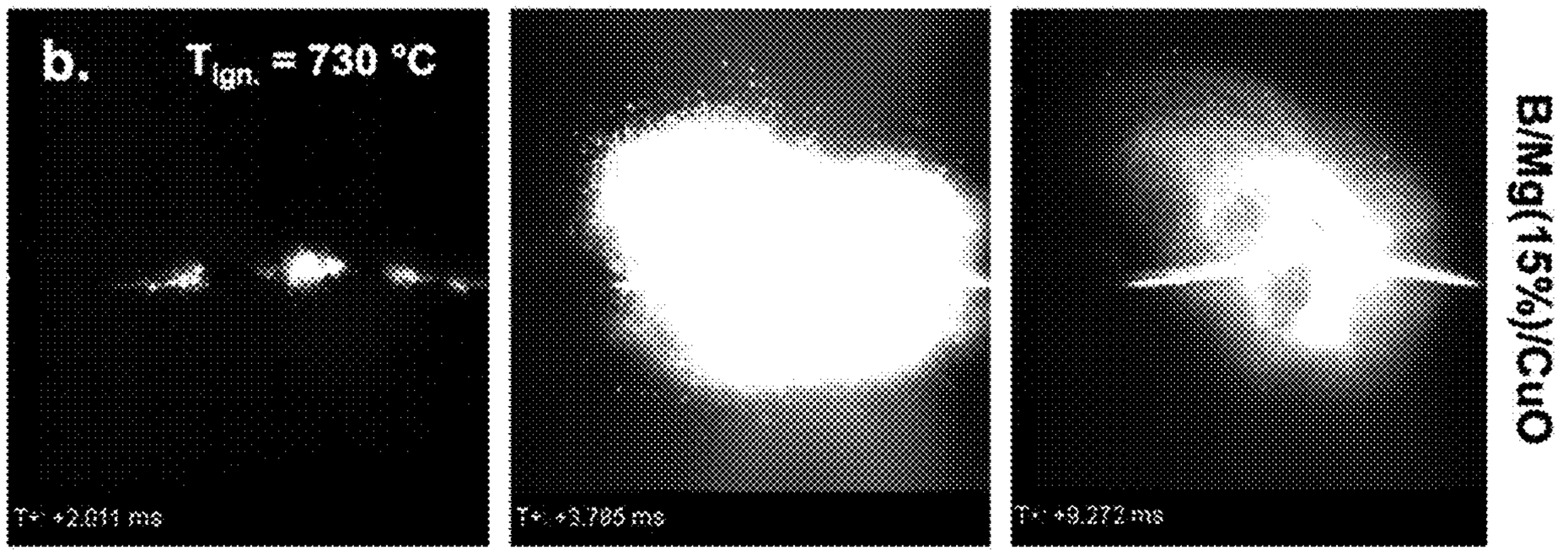

FIG. 14B

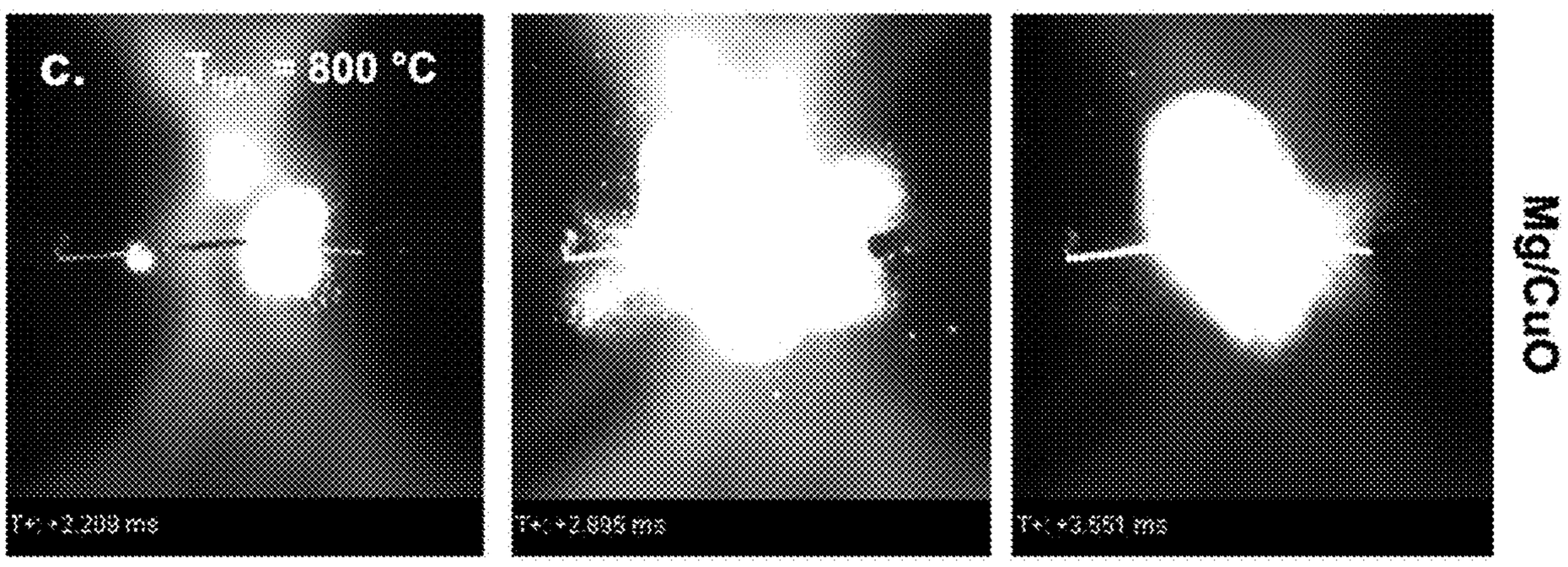

FIG. 14C

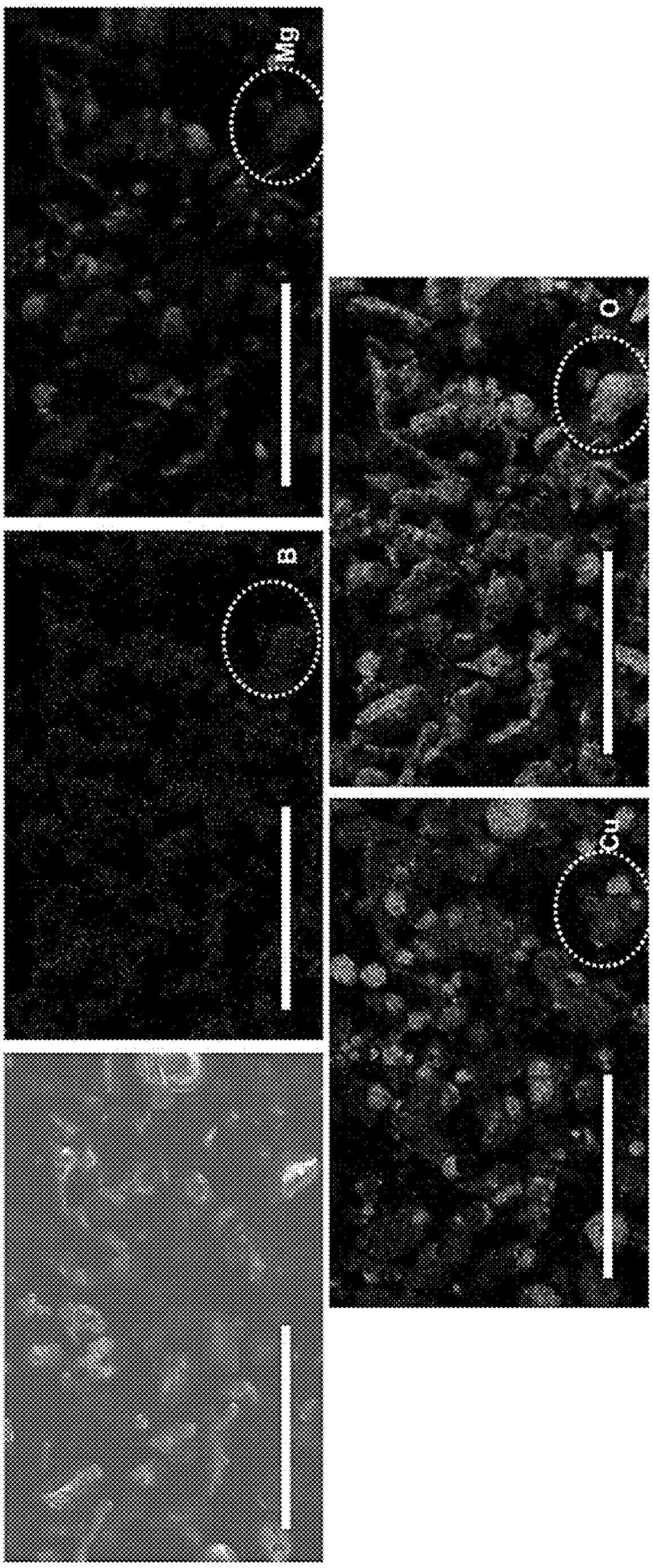

FIG. 15

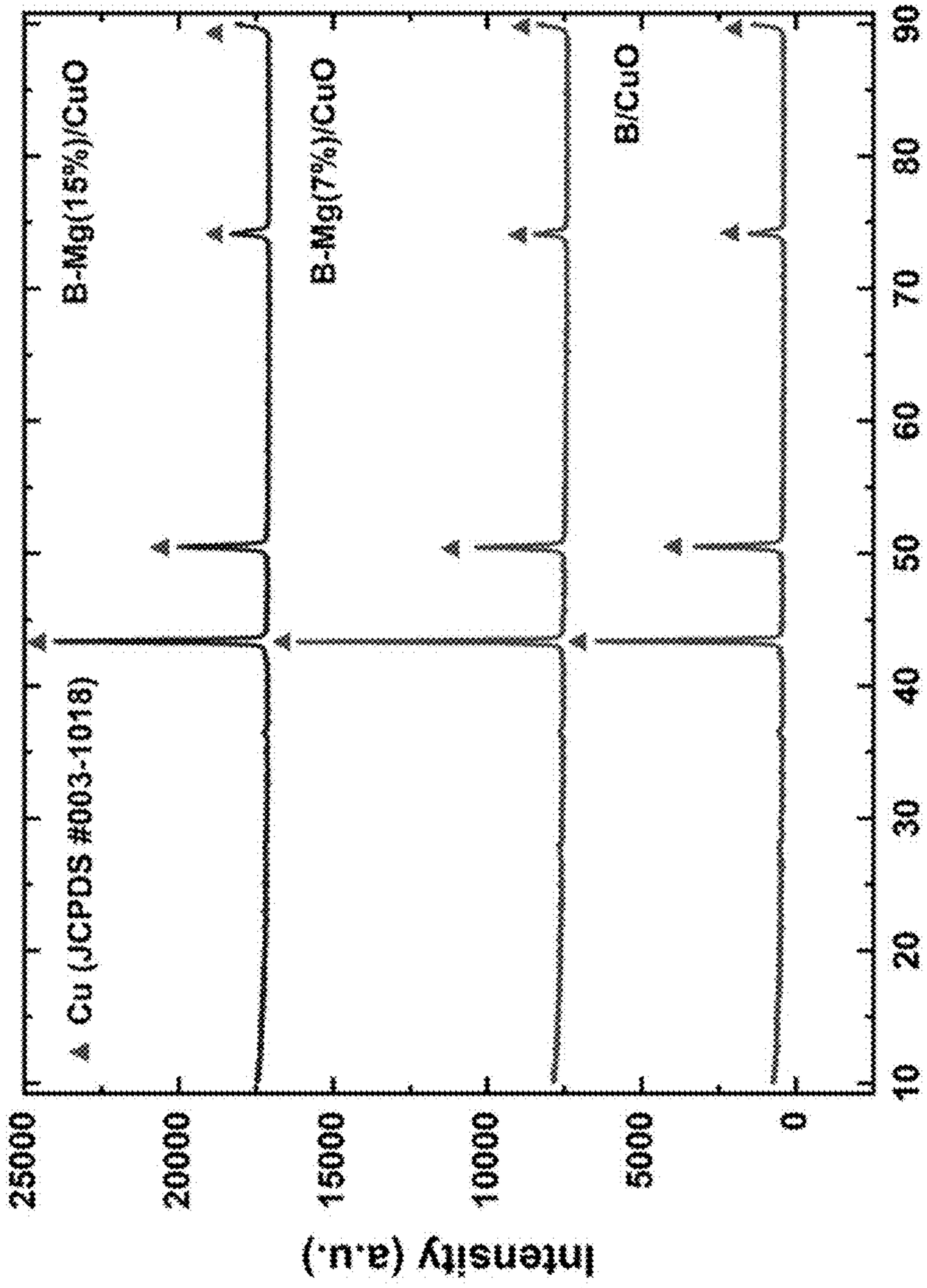
B-Mg(15%)/CuO
B-Mg(7%)/CuO
B/CuO
Cu (JCPDS #003-1018)
Intensity (a.u.)
Angle, 2θ (°)
25000
20000
15000
10000
5000
0
10
20
30
40
50
60
70
80
90

FIG. 16

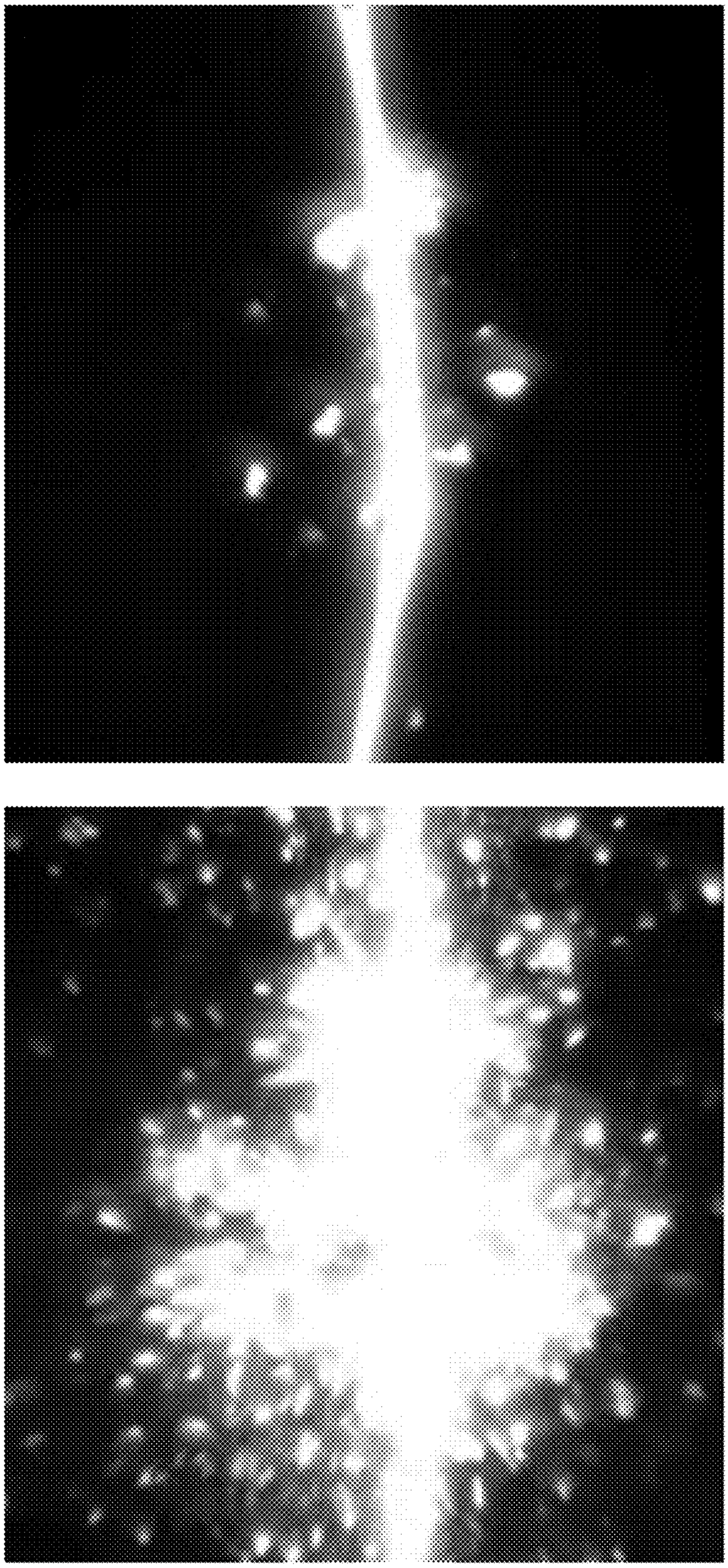

FIG. 17A

FIG. 17B

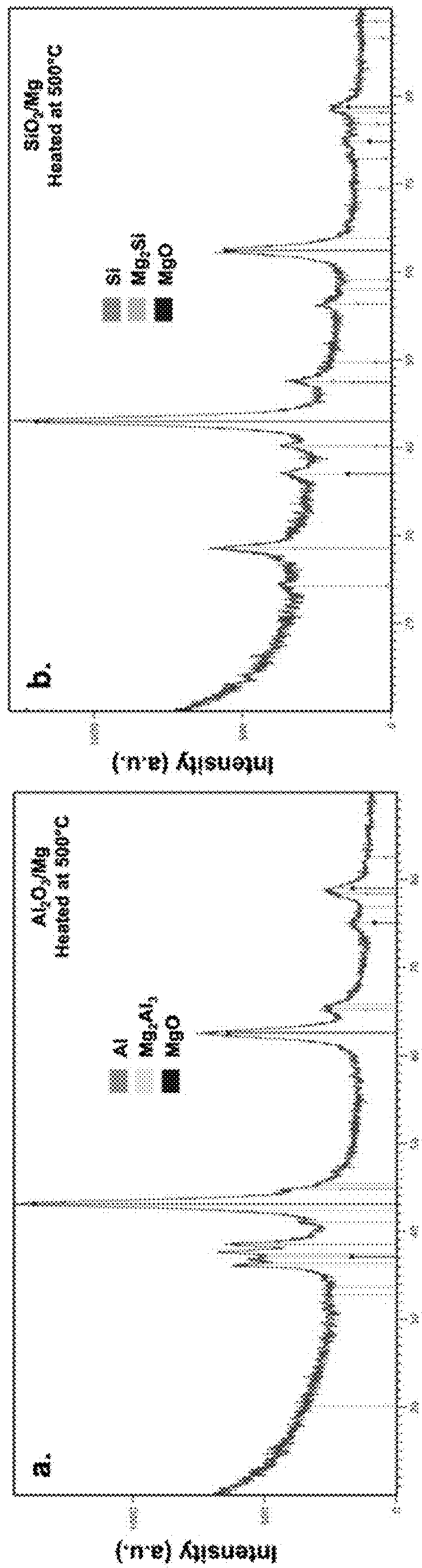

FIG. 18B

FIG. 18A

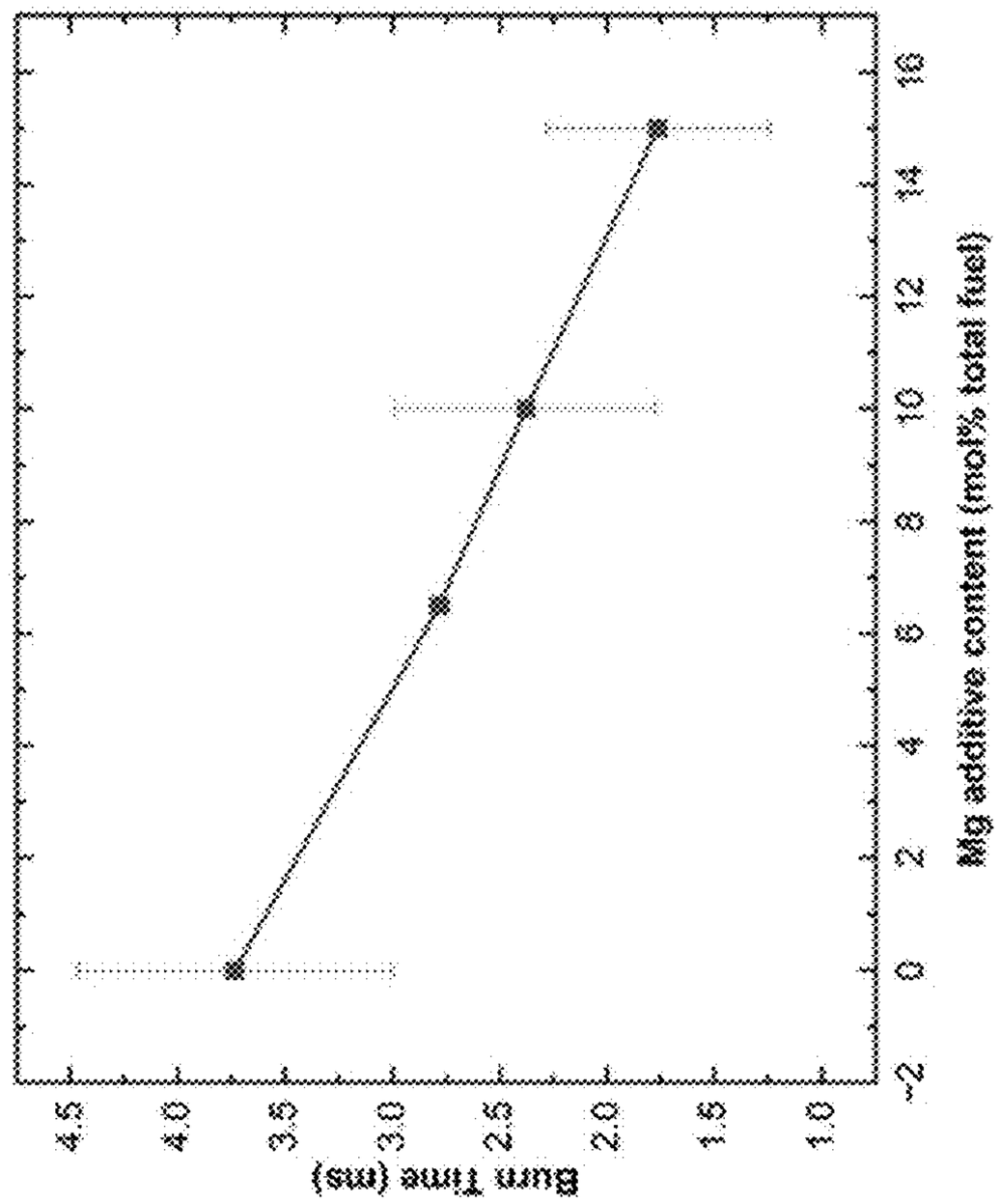

FIG. 19B

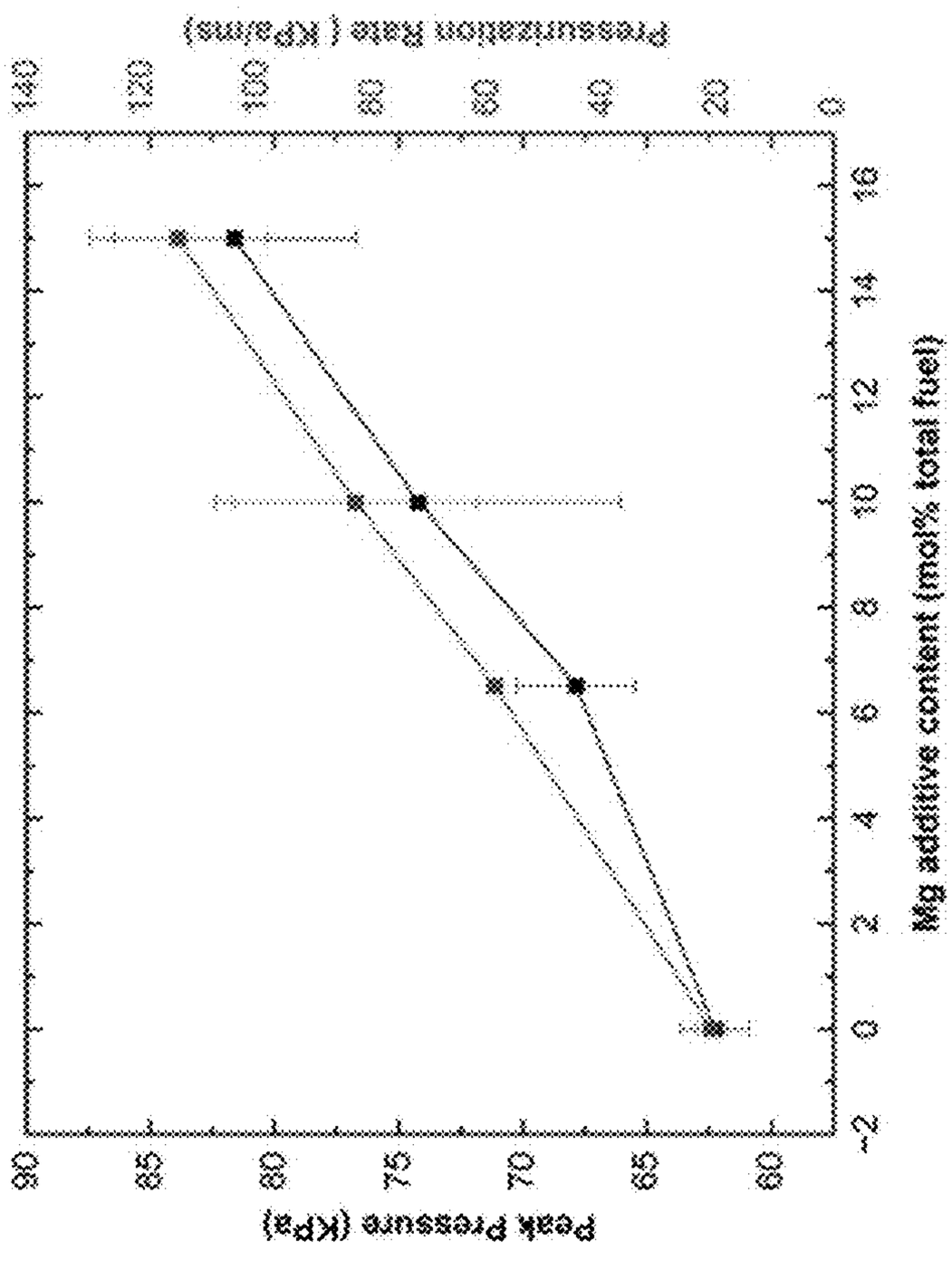

FIG. 19A

MAGNESIUM VAPOR INDUCED SURFACE DISRUPTION OF METAL PARTICLES

CROSS-REFERENCE TO RELATED APPLICATIONS

[0001] This patent document claims the benefits and priority to U.S. Provisional Patent Application No. 63/386,561, filed on Dec. 8, 2022, which is incorporated herein by reference in its entirety.

STATEMENT REGARDING FEDERALLY SPONSORED RESEARCH

[0002] This invention was made with government support under Contract No. N00014-21-1-2038 awarded by the Office of Naval Research. The Government has certain rights in the invention.

TECHNICAL FIELD

[0003] This patent document relates to material processing and engineering, and specifically to materials useful for energy storage.

BACKGROUND

[0004] Various nanoscale metals and metalloids have been explored as high-energy fuels in nanoenergetic composites for propellant and pyrotechnic applications.

SUMMARY

[0005] One aspect of the disclosure provided herein relates to a composition comprising magnesium nanoparticles, a nanoscale metal or metalloid, and an oxidizer. When compared to a second composition comprising the same amount of the oxidizer and the nanoscale metal or metalloid but without the magnesium nanoparticles, the composition may have one or more advantages selected from the following: a) a reduced burn time (e.g., reduced by about 50% to about 70%, and/or by about 2.0 ms to about 5.0 ms); b) an increased pressurization rate (e.g., increased by about 5-fold to about 6-fold); c) an increased peak pressure (e.g., increased by about 15% to about 30%); and d) a lower ignition temperature (e.g., lower by about 50° C. to about 200° C., and/or an ignition temperature of about 500° C. to about 750° C.).

[0006] Examples of the Metal or Metalloid Include, without Limitation, Boron, Silicon, Aluminum, and Titanium.

[0007] In some embodiments, the oxidizer comprises a first oxide of the metal or metalloid. For example, the first oxide of the metal or metalloid may be a native oxide shell of the metal or metalloid. In other examples, the first oxide of the metal or metalloid may further comprise oxides that are not the native oxide shell of the metal or metalloid.

[0008] In some embodiments, the oxidizer comprises one or more second oxides other than the oxides of the metal or metalloid. Examples of the one or more second oxides include, without limitation, CuO, B_2O_3, SiO_2, TiO_2, and Al_2O_3.

[0009] In some embodiments, the oxidizer may be oxygen.

[0010] In some embodiments, the nanoscale metal or metalloid has an average particle size of about 100 nm to about 900 nm, or about 390 nm to about 420 nm.

[0011] In some embodiments, the magnesium nanoparticles have an average particle size of about 100 nm to about 900 nm, or about 350 nm to about 400 nm.

[0012] In some embodiments, the molar of the magnesium nanoparticles over the total molar of the magnesium nanoparticles and the nanoscale metal or metalloid is no more than about 30%, no more than about 25%, no more than about 20%, nor more than about 15%, no more than about 10%, or about 3.0% to about 15.0%.

[0013] In some embodiments, the molar ratio of the nanoscale metal or metalloid over the oxidizer is about +/−20% of the stoichiometric ratio. In some embodiments, the molar ratio of the nanoscale metal or metalloid over the total molar of one or more second oxides is about +/−20% of the stoichiometric ratio.

[0014] In some embodiments, the molar ratio of the magnesium nanoparticles and nanoscale metal or metalloid over the oxidizer is about +/−20% of the stoichiometric ratio. In some embodiments, the molar ratio of the magnesium nanoparticles and nanoscale metal or metalloid over the total molar of one or more second oxides is about +/−20% of the stoichiometric ratio.

[0015] In some embodiments, the molar ratio of the oxidizer over the nanoscale metal or metalloid is about +/−20% of the stoichiometric ratio. In some embodiments, the molar ratio of the total molar of one or more second oxides over the nanoscale metal or metalloid is about +/−20% of the stoichiometric ratio.

[0016] In some embodiments, the molar ratio of the oxidizer over the magnesium nanoparticles and nanoscale metal or metalloid is about +/−20% of the stoichiometric ratio. In some embodiments, the molar ratio of the total molar of one or more second oxides over the magnesium nanoparticles and nanoscale metal or metalloid is about +/−20% of the stoichiometric ratio.

[0017] In some embodiments, the weight percent of the nanoscale metal or metalloid of the total weight of the composition is about 9.0% to about 10.5%.

[0018] In some embodiments, the weight percent of the magnesium nanoparticles of the total weight of the composition is about 0.5% to about 4.0%.

[0019] Another aspect of the disclosure provided herein relates to a method of fabricating the composition disclosed herein. The method comprises dispersing the magnesium nanoparticles, the nanoscale metal or metalloid, and the oxidizer in a first solvent to provide a first composition, and drying the first composition to provide the composition.

[0020] In some embodiments, the first solvent is an organic solvent that does not contain oxygen, or a mixture of multiple organic solvents that do not contain oxygen.

[0021] In some embodiments, the dispersing step comprises ultrasonication of the mixture to provide a homogeneous composition.

[0022] Techniques, systems and apparatus are described for fabricating magnesium-based composites. In particular, a composite includes a combination of magnesium nanoparticles and boron and/or copper oxide.

[0023] Those and other aspects and associated implementations and benefits of the disclosed technology are described in greater detail in the drawings, the description and the claims.

BRIEF DESCRIPTION OF THE DRAWINGS

[0024] This application contains at least one drawing executed in color. Copies of this application with color drawing(s) will be provided by the Office upon request and payment of the necessary fees.

[0025] FIG. **1**A shows comparison of volumetric and gravimetric energy density of boron with other fuels (Al, Mg, Si, and Ti) considering a stoichiometric reaction with the oxidizers oxygen. The energy density is calculated as the reaction enthalpy per unit mass or volume of the fuel.

[0026] FIG. **1**B shows comparison of volumetric and gravimetric energy density of boron with other fuels (Al, Mg, Si, and Ti) considering a stoichiometric reaction with the oxidizers CuO. The energy density is calculated as the reaction enthalpy per unit mass or volume of the fuel.

[0027] FIG. **2**A shows the effect of magnesium (Mg) addition on peak pressure and pressurization rate of boron/copper(II) oxide (B/CuO) nanoenergetic composites. Significant enhancement in peak pressure and pressurization were observed over B/CuO thermites, especially when the Mg mol % of total fuel (total molar of B and Mg) were about 7% or higher. The shaded area refers to compositions that showed significantly better performance over compositions without Mg.

[0028] FIG. **2**B shows the effect of magnesium (Mg) addition on burn characteristics of Mg/B/CuO composites. Significant reduction in burn times were observed over B/CuO thermites, especially when the Mg mol % of total fuel (total molar of B and Mg) were about 7% or higher. The shaded area refers to compositions that showed significantly better performance over compositions without Mg.

[0029] FIG. **3** shows a flowchart for a fabrication method of an embodiment of Mg/B/CuO composition as disclosed herein.

[0030] FIG. **4**A shows pressure (black) and optical traces (red) of the combustion of Mg with boron trioxide (B_2O_3) particles (simulant for the oxide shell of boron nanoparticles (B NP)).

[0031] FIG. **4**B shows snapshots of Mg/B_2O_3 ignition in argon (ignition temperature=600° C.) 2.692 ms (top panel) or 3.452 ms (bottom panel) after triggering.

[0032] FIG. **5**A shows thermogravimetric analysis (TGS in black) and differential scanning calorimetry (DSC in red) of magnesium nanoparticles (Mg NP) mixed with stoichiometric B_2O_3 (FIG. **5**A). Decomposition followed by an exothermic reduction of B_2O_3 particulates was shown.

[0033] FIG. **5**B shows x-ray diffraction (XRD) patterns of Mg/B_2O_3 samples heated at different temperatures (unheated, 350° C., 500° C., 650° C., and 1,000° C.), with the magnesiothermic reduction of B_2O_3 occurring ~500-650° C.

[0034] FIG. **6** shows attenuated total reflection Fourier transform infrared (ATR-FTIR) spectra of neat B_2O_3 (green), unheated Mg/B_2O_3 composites (red), and Mg/B_2O_3 samples heated at 650° C.(purple).

[0035] FIG. **7**A shows high speed time of flight mass spectrometry (T-jump/TOFMS) spectrum showing H_2O, HOBO, and vapor-phase Mg species evolved from rapid heating of Mg/B_2O_3.

[0036] FIG. **7**B shows temporal evolution of different species evolved from the Mg/B_2O_3 reaction as obtained from T-jump/TOFMS, m/z of 18 (dark blue), 24 (green), 45 (red), and 62 (light blue).

[0037] FIG. **8** shows DSC of Mg/B_2O_3 (red) and Mg/B (blue) mixtures in argon, showing coinciding exothermic peaks of Mg/B and Mg/B_2O_3 reaction exotherms. The Mg/B sample represents ~10 mol % Mg with respect to the total mixture.

[0038] FIG. **9**A proposed a hypothetical Mg vapor-induced mechanism of the Mg/B_2O_3 reaction.

[0039] FIG. **9**B proposed a hypothetical Mg-vapor induced oxide etching and removal mechanism for boron nanoparticles (B NPs) that may be responsible for reactivity enhancement.

[0040] FIG. **10**A shows scanning electron microscope (SEM) images of as-received B NPs (mean particle size ~410 nm). Scale bars: 5 μm.

[0041] FIG. **10**B shows scanning electron microscope (SEM) images of Mg NPs synthesized by electromagnetic levitation (mean particle size ~370 nm). Scale bars: 5 μm.

[0042] FIG. **11**A shows TGA traces of B NPs in O_2 atmosphere (initial heating rate=10° C./min to 1200° C., followed by isothermal oxidation at 1200° C.).

[0043] FIG. **11**B shows TGA traces of Mg NPs in air at a heating rate of 10° C./min.

[0044] FIG. **12** shows SEM images of B_2O_3 particles (simulant for the oxide layer, B_2O_3, of boron NPs) obtained after ball milling. Scale bar: 20 μm.

[0045] FIG. **13**A shows pressure profiles obtained from constant-volume combustion cell characterization of B/Mg/CuO composites at various Mg mol %, 0.0% (black), 3.0% (red), 6.6% (brown), 10.0% (green), and 15.0% (purple).

[0046] FIG. **13**B shows optical emission profiles obtained from constant-volume combustion cell characterization of B/Mg/CuO composites at various Mg mol %, 0.0% (black), 3.0% (red), 6.6% (brown), 10.0% (green), and 15.0% (purple).

[0047] FIG. **14**A shows ignition snapshot of B/CuO in an argon atmosphere, 2.122 ms (left), 4.895 ms (middle), and 8.832 ms (right) after triggering.

[0048] FIG. **14**B shows ignition snapshot of B/Mg(15%)/CuO in an argon atmosphere, 2.011 ms (left), 3.785 ms (middle), and 9.272 ms (right) after triggering.

[0049] FIG. **14**C shows ignition snapshot of Mg/CuO in an argon atmosphere, 2.209 ms (left), 2.895 ms (middle), and 3.551 ms (right) after triggering.

[0050] FIG. **15** shows scanning electron microscope-energy dispersive X ray spectroscopy (SEM-EDS) maps of reaction products collected from the combustion of B/Mg (15%)/CuO. Scale bar: 250 μm.

[0051] FIG. **16** shows XRD patterns of reaction products collected from the combustion of an embodiment of B/CuO composition (bottom, black), an embodiment of B—Mg (7%)/CuO composition (middle, red) and an embodiment of B—Mg (15%)/CuO composition (top, blue).

[0052] FIG. **17**A shows violent reaction of Mg NPs with titanium dioxide nanoparticles (TiO_2 NP) in Ar, suggesting that Mg can react with the oxide surfaces of titanium (Ti).

[0053] FIG. **17**B shows violent reaction of Mg NPs with silicon dioxide nanoparticles (SiO_2 NP) in Ar, suggesting that Mg can react with the oxide surfaces of silicon (Si).

[0054] FIG. **18**A shows XRD patterns of products collected from heating Al_2O_3/Mg at 500° C., showing the formation of zerovalent Al (green) along with alloyed products (Mg_2Al_3, yellow) and MgO (blue).

[0055] FIG. **18**B shows XRD patterns of products collected from heating SiO_2/Mg at 500° C., showing the formation of zerovalent Si (green) along with alloyed products (Mg_2Si, grey), and MgO (blue).

[0056] FIG. **19**A shows pressurization rate (red) and peak pressure (black) of Mg—Ti/CuO thermite mixtures with various Mg mol % total fuel, which showed enhancement effects from Mg addition.

[0057] FIG. **19**B shows burn characteristics of Mg—Ti/CuO thermite mixtures with various Mg mol % total fuel, which showed enhancement effects from Mg addition to Ti/CuO composites.

DETAILED DESCRIPTION

[0058] As used in the specification and claims, the singular form "a," "an," and "the" includes plural references unless the context clearly dictates otherwise. It should be understood that the terms "a" and "an" as used herein refer to "one or more" of the enumerated components.

[0059] The use of the alternative (e.g., "or") should be understood to mean either one, both, or any combination thereof of the alternatives.

[0060] The term "about" as used herein in the context of a number refers to a range centered on that number and spanning 10% less than that number and 10% more than that number. The term "about" used in the context of a range refers to an extended range spanning 10% less than that the lowest number listed in the range and 10% more than the greatest number listed in the range.

[0061] Throughout this disclosure, any concentration range, percentage range, ratio range, or integer range is to be understood to include the value of any integer within the recited range and, when appropriate, fractions thereof (such as one tenth and one hundredth of an integer), unless otherwise indicated. Also, any number range of this disclosure relating to any physical feature, such as polymer subunits, size, or thickness, are to be understood to include any integer within the recited range, unless otherwise indicated. Throughout this disclosure, numerical ranges are inclusive of their recited endpoints, unless specifically stated otherwise.

[0062] Unless the context requires otherwise, throughout the present specification and claims, the word "comprise" and variations thereof, such as, "comprises" and "comprising" are to be construed in an open, inclusive sense, that is, as "including, but not limited to." As used herein, the terms "include" and "comprise" are used synonymously.

[0063] Unless specified otherwise, the terms "composition" and "composite" may be used interchangeably.

[0064] Unless specified otherwise, the term "fuel" refers to the metal and metalloid of a composition disclosed herein. For example, for a composition comprising Mg nanoparticles, a nanoscale metal or metalloid, and an oxidizer, the term "fuel" refers to Mg nanoparticles and the nanoscale metal or metalloid.

[0065] Nanoscale metals and metalloids such as aluminum (Al), titanium (Ti), magnesium (Mg), boron (B), and silicon (Si), have been explored as high-energy fuels in nanoenergetic composites for propellant and pyrotechnic applications. Among these fuels, boron is regarded as the premier candidate fuel due to its higher gravimetric and volumetric reaction enthalpies, as shown in FIGS. **1**A and **1**B. Despite its thermodynamic advantages over other fuels, boron suffers from sluggish oxidation and energy release kinetics due to its low-melting oxide shell (B_2O_3, melting point ~450° C.). Post melting, the non-volatile liquid oxide layer (boiling point ~1,860° C.)acts as a diffusion barrier to the oxidizing species and restricts their access to the B core, thereby significantly inhibiting B oxidation and energy release.

[0066] As shown in the Examples provided herein, the incorporation of Mg nanoparticles (NPs) in embodiments of boron/copper(II) oxide (B/CuO) thermite compositions (Example 1) and in Ti/CuO thermite compositions (Example 3) both resulted in higher reactivities. For example, when compared to the corresponding thermite compositions without Mg NPs, the pressurization rates of the Mg-present thermite compositions were enhanced to about 6-fold higher (FIG. **2**A for Mg—B/CuO) or about 5-fold higher (FIG. **19**A for Mg—Ti/CuO), and the burn times were reduced to about 70% (FIG. **2**B for Mg—B/CuO, from about 6.5 mg to about 2 ms) or about 54% (FIG. **19**B for Mg—Ti/CuO, from about 3.7 ms to about 1.7 ms). More specifically, embodiments of B/CuO composites with Mg NPs (~370 nm) incorporated as an additive fuel with loadings ranging from ~3-15 mol % of the total fuel were fabricated (Table 1) and evaluated; and embodiments of Ti/CuO composites with Mg NPs (~370 nm) incorporated as an additive fuel with loadings ranging of about 6.6%, about 10%, and about 15 mol % of the total fuel were fabricated and evaluated, the Ti/CuO mass ratio was kept constant at phi=1 as the stoichiometric ratio. The considerable enhancement in the pressurization and reduction in the burning times suggested that adding Mg to B-based or Ti-based composites augmented their reaction kinetics. Mg-based composites (without B or Ti) fabricated with the highest additive Mg amount tested (15 mol %) did not ignite or show pressurization with CuO. This was expected, since from a compositional perspective, these composites were fuel-lean since Mg was only a minor, additive fuel in these composites.

[0067] The mechanism of the reaction between Mg and B_2O_3 particles was probed through a combination of differential scanning calorimetry (DSC), reaction product characterization, and high-speed time-of-flight mass spectrometry (T-jump/TOFMS). These characterizations revealed that the mechanism of the Mg—B_2O_3 interaction may involve an exothermic redox reaction between vapor-phase Mg and molten B_2O_3, without wishing to be bound by the mechanism. For example, Mg vapor may undergo one or more heterogeneous reactions with molten B_2O_3 shell of boron at relatively low temperatures. These surface reactions may occur prior to the ignition of B with CuO and may cause surface disruptions in the oxide shell, resulting in the observed enhanced reactivity of B-composites, without wishing to be bound by the mechanism.

[0068] Magnesium nanoparticles also showed similar exothermic redox reactions with Al_2O_3, TiO_2, and SiO_2 (Table 3). Adding Mg to other nanoscale fuels (e.g., Al, and Si) may also result in a similar enhancement in their energy release by reacting with their oxide shell.

[0069] Magnesium nanoparticles, as an additive fuel, may offer a thermodynamically and kinetically viable source of a highly reactive gas-phase Mg that can potentially act as an etchant for the oxide shell of metal or metalloid in a thermite composition, without wishing to be bound by the mechanism.

[0070] One aspect of the disclosure provided herein relates to a composition comprising magnesium nanoparticles, a nanoscale metal or metalloid, and an oxidizer. When compared to a second composition comprising the same amount of the oxidizer and the nanoscale metal or metalloid but without the magnesium nanoparticles, the composition may

have one or more advantages selected from the following: a) a reduced burn time (e.g., reduced by about 50% to about 70%, and/or by about 2.0 ms to about 5.0 ms); b) an increased pressurization rate (e.g., increased by about 5-fold to about 6-fold); c) an increased peak pressure (e.g., increased by about 15% to about 30%); and d) a lower ignition temperature (e.g., an ignition temperature of about 500° C. to about 750° C.).

[0071] Examples of the metal or metalloid include, without limitation, boron, silicon, aluminum, and titanium.

[0072] In some embodiments, the composition comprises magnesium nanoparticles, a nanoscale metal or metalloid, and an oxidizer, wherein the composition has a burn time reduced by about 50% to about 70% when compared to a second composition comprising the same amount of the oxidizer and the nanoscale metal or metalloid but without the magnesium nanoparticles. In certain embodiments, the burn time is reduced by about 1.0 ms to about 10.0 ms, about 1.5 ms to about 10.0 ms, about 2.0 ms to about 10.0 ms, about 2.5 ms to about 10.0 ms, about 3.0 ms to about 10.0 ms, about 3.5 ms to about 10.0 ms, about 4.0 ms to about 10.0 ms, about 4.5 ms to about 10.0 ms, about 5.0 ms to about 10.0 ms, about 5.5 ms to about 10.0 ms, about 6.0 ms to about 10.0 ms, about 6.5 ms to about 10.0 ms, about 7.0 ms to about 10.0 ms, about 1.0 ms to about 9.0 ms, about 1.5 ms to about 9.0 ms, about 2.0 ms to about 9.0 ms, about 2.5 ms to about 9.0 ms, about 3.0 ms to about 9.0 ms, about 3.5 ms to about 9.0 ms, about 4.0 ms to about 9.0 ms, about 4.5 ms to about 9.0 ms, about 5.0 ms to about 9.0 ms, about 5.5 ms to about 9.0 ms, about 6.0 ms to about 9.0 ms, about 6.5 ms to about 9.0 ms, about 7.0 ms to about 9.0 ms, about 1.0 ms to about 8.0 ms, about 1.5 ms to about 8.0 ms, about 2.0 ms to about 8.0 ms, about 2.5 ms to about 8.0 ms, about 3.0 ms to about 8.0 ms, about 3.5 ms to about 8.0 ms, about 4.0 ms to about 8.0 ms, about 4.5 ms to about 8.0 ms, about 5.0 ms to about 8.0 ms, about 5.5 ms to about 8.0 ms, about 6.0 ms to about 8.0 ms, about 6.5 ms to about 8.0 ms, about 7.0 ms to about 8.0 ms, about 1.0 ms to about 7.0 ms, about 1.5 ms to about 7.0 ms, about 2.0 ms to about 7.0 ms, about 2.5 ms to about 7.0 ms, about 3.0 ms to about 7.0 ms, about 3.5 ms to about 7.0 ms, about 4.0 ms to about 7.0 ms, about 4.5 ms to about 7.0 ms, about 5.0 ms to about 7.0 ms, about 5.5 ms to about 7.0 ms, about 6.0 ms to about 7.0 ms, about 1.0 ms to about 8.5 ms, about 1.0 ms to about 7.5 ms, about 2.0 ms to about 5.0 ms, about 4.5 ms, or about 2 ms. In certain embodiments, the burn time is reduced by at least about 10%, at least about 20%, at least about 30%, at least about 40%, at least about 50%, at least about 60%, at least about 70%, at least about 80%, at least about 90%, or any ranges there between.

[0073] In some embodiments, the composition comprises magnesium nanoparticles, a nanoscale metal or metalloid selected from the group consisting of boron, silicon, aluminum, and titanium, and an oxidizer, wherein the composition has a pressurization rate increased by about 5 fold to about 6 fold when compared to a second composition comprising the same amount of the oxidizer and the nanoscale metal or metalloid but without the magnesium nanoparticles. In certain embodiments, the pressurization rate is increased by at least about 1 fold, at least about 2 fold, at least about 3 fold, at least about 4 fold, at least about 5 fold, at least about 6 fold, at least about 7 fold, at least about 8 fold, at least about 9 fold, at least about 10 fold, or any ranges therebetween.

[0074] In some embodiments, the composition comprises magnesium nanoparticles, a nanoscale metal or metalloid selected from the group consisting of boron, silicon, aluminum, and titanium, and an oxidizer, wherein the composition has a peak pressure increased by about 15% to about 30% when compared to a second composition comprising the same amount of the oxidizer and the nanoscale metal or metalloid but without the magnesium nanoparticles. In certain embodiments, the peak pressure is increased by at least about 5%, at least about 10%, at least about 15%, at least about 20%, at least about 25%, at least about 30%, at least about 35%, at least about 40%, or any ranges therebetween.

[0075] In some embodiments, the composition comprises magnesium nanoparticles, a nanoscale metal or metalloid selected from the group consisting of boron, silicon, aluminum, and titanium, and an oxidizer, wherein the composition has a lower ignition temperature when compared to a second composition comprising the same amount of the oxidizer and the nanoscale metal or metalloid but without the magnesium nanoparticles. In certain embodiments, the ignition temperature is lowered by at least about 50° C., at least about 75° C., at least about 100° C., at least about 125° C., at least about 150° C., at least about 175° C., at least about 200° C., or any ranges therebetween. In certain embodiments, the ignition temperature is about 500° C. to about 750° C., lower than about 750° C., lower than about 700° C., lower than about 650° C., lower than about 600° C., lower than about 550° C., or about 500° C., or any ranges therebetween.

[0076] In some embodiments, the oxidizer comprises a first oxide of the metal or metalloid. In some embodiments, the first oxide of the metal or metalloid is a native oxide shell of the metal or metalloid. In some embodiments, the first oxide of the metal or metalloid may further comprise oxides that are not the native oxide shell of the metal or metalloid.

[0077] In some embodiments, the oxidizer comprises one or more second oxides other than the oxides of the metal or metalloid. Examples of the one or more second oxides include, without limitation, CuO, B_2O_3, SiO_2, TiO_2, and Al_2O_3.

[0078] In some embodiments, the oxidizer may be oxygen.

[0079] In some embodiments, the nanoscale metal or metalloid has an average particle size of no more than about 100 nm, no more than about 120 nm, no more than about 140 nm, no more than about 160 nm, no more than about 180 nm, no more than about 200 nm, no more than about 220 nm, no more than about 240 nm, no more than about 260 nm, no more than about 280 nm, no more than about 300 nm, no more than about 310 nm, no more than about 320 nm, no more than about 330 nm, no more than about 340 nm, no more than about 350 nm, no more than about 360 nm, no more than about 370 nm, no more than about 380 nm, no more than about 390 nm, no more than about 400 nm, no more than about 410 nm, no more than about 420 nm, no more than about 430 nm, no more than about 440 nm, no more than about 450 nm, no more than about 475 nm, no more than about 500 nm, no more than about 525 nm, no more than about 550 nm, no more than about 575 nm, no more than about 600 nm, no more than about 650 nm, no more than about 700 nm, no more than about 750 nm, no more than about 800 nm, no more than about 850 nm, no more than about 900 nm, no more than about 950 nm, no more than about 1000 nm, or any combination of values establishing a range thereof. For example, in some embodi-

ments, the nanoscale metal or metalloid has an average particle size of about 390 nm to about 420 nm.

[0080] In some embodiments, the magnesium nanoparticles have an average particle size of no more than about 100 nm, no more than about 120 nm, no more than about 140 nm, no more than about 160 nm, no more than about 180 nm, no more than about 200 nm, no more than about 220 nm, no more than about 240 nm, no more than about 260 nm, no more than about 280 nm, no more than about 300 nm, no more than about 310 nm, no more than about 320 nm, no more than about 330 nm, no more than about 340 nm, no more than about 350 nm, no more than about 360 nm, no more than about 370 nm, no more than about 380 nm, no more than about 390 nm, no more than about 400 nm, no more than about 410 nm, no more than about 420 nm, no more than about 430 nm, no more than about 440 nm, no more than about 450 nm, no more than about 475 nm, no more than about 500 nm, no more than about 525 nm, no more than about 550 nm, no more than about 575 nm, no more than about 600 nm, no more than about 650 nm, no more than about 700 nm, no more than about 750 nm, no more than about 800 nm, no more than about 850 nm, no more than about 900 nm, no more than about 950 nm, no more than about 1000 nm, or any combination of values establishing a range thereof. For example, in some embodiments, the magnesium nanoparticles have an average particle size of about 350 nm to about 400 nm.

[0081] In some embodiments, the molar of the magnesium nanoparticles over the total molar of the magnesium nanoparticles and the nanoscale metal or metalloid ranges is at least about 1.5%, at least about 2.0%, at least about 2.5%, at least about 3.0%, at least about 3.5%, at least about 4.0%, at least about 4.5%, at least about 5.0%, at least about 6.0%, at least about 7.0%, at least about 8.0%, at least about 9.0%, at least about 10.0%, at least about 11.0%, at least about 12.0%, at least about 13.0%, at least about 14.0%, at least about 15.0%, at least about 16.0%, at least about 17.0%, at least about 18.0%, at least about 19.0%, at least about 20.0%, at least about 21.0%, at least about 22.0%, at least about 23.0%, at least about 24.0%, at least about 25.0%, at least about 26.0%, at least about 27.0%, at least about 28.0%, at least about 29.0%, at least about 30.0%, or any combination of values establishing a range thereof. For example, in some embodiments, the molar of the magnesium nanoparticles over the total molar of the magnesium nanoparticles and the nanoscale metal or metalloid is about 3.0% to about 15.0%.

[0082] In some embodiments, the molar ratio of the nanoscale metal or metalloid over the oxidizer is about +/−20%, about +/−15%, about +/−10%, or about +/−5% of the stoichiometric ratio. In some embodiments, the molar ratio of the nanoscale metal or metalloid over the total molar of one or more second oxides is about +/−20%, about +/−15%, about +/−10%, or about +/−5% of the stoichiometric ratio.

[0083] In some embodiments, the molar ratio of the magnesium nanoparticles and nanoscale metal or metalloid over the oxidizer is about +/−20%, about +/−15%, about +/−10%, or about +/−5% of the stoichiometric ratio. In some embodiments, the molar ratio of the magnesium nanoparticles and nanoscale metal or metalloid over the total molar of one or more second oxides is about +/−20% of the stoichiometric ratio.

[0084] In some embodiments, the molar ratio of the oxidizer over the nanoscale metal or metalloid is about +/−20%, about +/−15%, about +/−10%, or about +/−5% of the stoichiometric ratio. In some embodiments, the molar ratio of the total molar of one or more second oxides over the nanoscale metal or metalloid is about +/−20%, about +/−15%, about +/−10%, or about +/−5% of the stoichiometric ratio.

[0085] In some embodiments, the molar ratio of the oxidizer over the magnesium nanoparticles and nanoscale metal or metalloid is about +/−20%, about +/−15%, about +/−10%, or about +/−5% of the stoichiometric ratio. In some embodiments, the molar ratio of the total molar of one or more second oxides over the magnesium nanoparticles and nanoscale metal or metalloid is about +/−20% of the stoichiometric ratio.

[0086] In some embodiments, the weight percent of the nanoscale metal or metalloid of the total weight of the composition is about 9.0% to about 10.5%.

[0087] In some embodiments, the weight percent of the magnesium nanoparticles of the total weight of the composition is about 0.5% to about 4.0%.

[0088] Another aspect of the disclosure provided herein relates to a method of fabricating the composition disclosed herein.

[0089] In certain embodiments, the method comprises dispersing the magnesium nanoparticles, the nanoscale metal or metalloid, and the oxidizer in a first solvent to provide a first composition, and drying the first composition to provide the composition.

[0090] In some embodiments, the first solvent is an organic solvent that does not contain oxygen, or a mixture of multiple organic solvents that do not contain oxygen. Examples of the first solvent includes, without limitation, aliphatic hydrocarbons (e.g., alkanes, alkenes, and alkynes), aromatic hydrocarbons (e.g., benzene, toluene), hydrocarbons substituted with one or more halogens (e.g., F, Cl, Br, I), such as dichloromethane, chloroform, and hydrocarbons substituted with one or more amino groups. In some embodiments, the first solvent is hexane.

[0091] In some embodiments, the dispersing step comprises ultrasonication of the mixture to provide a homogeneous composition.

[0092] In certain embodiments, the method comprises incorporating Mg nanoparticles into a third composition comprising the nanoscale metal or metalloid and the oxidizer.

[0093] One specific embodiment of the fabrication process **300** is depicted in FIG. **3**. First, a boron-copper oxide composite is prepared (**302**). Next, Mg nanoparticles are introduced into the composite as described herein (**304**). The resulting composite material is used for further experiments and end uses.

EXAMPLES

[0094] The following examples are intended to illustrate various embodiments of the invention. As such, the specific embodiments discussed are not to be constructed as limitations on the scope of the invention. It will be apparent to one skilled in the art that various equivalents, changes, and modifications may be made without departing from the scope of invention, and it is understood that such equivalent embodiments are to be included herein. Further, all references cited in the disclosure are hereby incorporated by

reference in their entirety, as if fully set forth herein, to the extent that they do not contradict or are not inconsistent with the instant disclosure.

Example 1: Magnesium-Enhanced Reactivity of Boron Particles: Role of Mg/B_2O_3 Exothermic Surface Reactions

[0095] Boron has offered great promise as a candidate fuel in high-energy composites due to its high gravimetric and volumetric energy content, however, its oxidation rate is limited by sluggish diffusion of reactive species across its low-melting oxide shell. On the other hand, Mg nanoparticles (NPs) have been shown recently to undergo rapid vaporization (~100 us). This release of vapor-phase Mg can potentially be exploited to react exothermically (AH_r=−420 KJ/mol) with the B_2O_3 layer on boron, aiding in surface disruption. Mg NPs were evaluated as an additive fuel to B/CuO nanoenergetic composites. The incorporation of Mg as an additive fuel in B/CuO composites yielded a ~6-fold enhancement in reactivity with a ~60% reduction in burn time. Through thermal and reaction product analysis along with high-speed mass spectrometry (T-jump/TOFMS) and ignition characterization, the reaction mechanism of Mg/B_2O_3 particles as a simulant system for the interaction of Mg with the B_2O_3 shell of boron was investigated. These characterizations revealed that exothermic heterogeneous reactions occur between vapor-phase Mg and molten B_2O_3 shell of boron at ~500-650° C.

[0096] Nanoscale metals and metalloids such as Al, Ti, Mg, B, and Si, have been explored as high-energy fuels in nanoenergetic composites for propellant and pyrotechnic applications. Among these fuels, boron has always been regarded as the premier candidate fuel due to its higher gravimetric and volumetric reaction enthalpies, as shown in FIGS. **1**A and **1**B. Despite its thermodynamic advantages over other fuels, boron suffers from sluggish oxidation and energy release kinetics due to its low-melting oxide shell (B_2O_3, melting point ~450° C.). Post melting, the non-volatile liquid oxide layer (boiling point ~1860° C.) acts as a diffusion barrier to the oxidizing species and restricts their access to the B core, thereby significantly inhibiting B oxidation and energy release. Several surface modification strategies such as oxide removal by solvent washing, surface functionalization with fluorine-based organic, polymeric, and graphitic moieties, and incorporation of fluoride salts, have been explored to alter or remove the oxide surface of boron to promote its ignition and combustion characteristics.

[0097] Binary fuel systems were explored through the incorporation of energy-dense metal additives such as Al, Mg, and Ti, in boron powders to accelerate B oxidation while maintaining a high energetic content. Employing similar dual fuel systems has been used to control and modulate the transport processes and ignition in thermite mixtures. Among the metal additives explored so far, Mg is particularly attractive due to its high volatility and reactivity. Reducing particle size of Mg NPs could result in their rapid vaporization and a fast vapor-phase Mg release (release timescale ~ 100 μs at a heating rate of 10^{5}° C./s). Additionally, due to the highly negative formation energies of MgO compared to B_2O_3 (Mg lies lower than B in the Ellingham diagram), the reaction between Mg and B_2O_3 may be thermodynamically feasible with a reaction enthalpy (AH_r) of ~−420 KJ/mol or −2.9 KJ/g. Mg NPs, as an additive fuel, was tested to offer a thermodynamically and kinetically viable source of a highly reactive gas-phase Mg that may potentially act as an etchant for the oxide shell of boron according to the following reaction:

$$3Mg+B_2O_3 \rightarrow 3MgO+B, \Delta H_r = -420 \text{ kj/mol}_{reaction}$$

[0098] Previous studies have reported that coating boron with materials (e.g., fluorographene and fluoroalkylsilanes) that can release gas-phase fluorine species to etch with the B_2O_3 shell promotes its ignition and combustion. Without wishing to be bound by the mechanism, nanoscale Mg tested herein appeared to provide advantages by generating reactive gas-phase species (Mg vapor) to corrode the oxide shell while maintaining a high energy density of the composites. Although prior studies have explored the role of Mg as an additive in B-based powders, those reports were limited to micron-scale Mg powders that, due to their low surface area, may have slow vaporization and release kinetics of gas-phase Mg species. Furthermore, it was unexpected to observe the synergistic effects of the surface reaction of Mg vapor directly with the oxide shell of boron provided herein.

[0099] The energy release characteristics of B/CuO composites with Mg NPs (~370 nm) incorporated as an additive fuel with loadings ranging from ~3-15 mol % of the total fuel were fabricated and evaluated. It was demonstrated that incorporating Mg in B/CuO thermite resulted in up to 6-fold higher pressurization rates and ~60% reduction in burn times of the composites. Through a combination of differential scanning calorimetry (DSC), reaction product characterization, and high-speed time-of-flight mass spectrometry (T-jump/TOFMS), the mechanism of the reaction between Mg and B_2O_3 particles was probed. These characterizations revealed that the mechanism of the Mg—B_2O_3 interaction involves an exothermic redox reaction between vapor-phase Mg and molten B_2O_3.

Materials

[0100] Boron (~410 nm as measured from the SEM in FIG. **10**A, 80% active B content) and copper oxide nanoparticles (CuO, ~40 nm) were obtained from US Research Nanomaterials. For boron etching studies, Mg NPs were prepared by an electromagnetic levitation technique as described in Ghildiyal et al. ACS Appl. Mater. Interfaces 14(15) 17164-17174, 2022. Briefly, a ~0.35 g spheroidal Mg piece was levitated and heated up to ~993K in a purified Ar/He gas flow. Mg NPs were recovered downstream from the particle-laden gas on a Millipore Sigma polycarbonate membrane filter (0.3 μm pore diameter). The average particle size of the synthesized Mg NPs was ~370 nm, as shown in FIG. **10**B, while the active Mg content was estimated to be ~88%. The active content of the fuels (B and Mg) were estimated from the mass gain upon oxidation in air or O_2.

[0101] The active content of B NPs was determined by performing TGA in an O_2 atmosphere at 1200° C. for ~80 min, as shown in FIG. **11**A. The high temperature and O_2 atmosphere were employed to ensure complete oxidation of B. Similarly, TGA was also used to determine the active metallic content in Mg particles. However, for Mg, air was employed (FIG. **11**B) as the atmosphere since the particles were sensitive to ignition in pure O_2. For both fuels, the mass gain in the TGA curve was assumed primarily due to the formation of oxides (B_2O_3/MgO), according to the following reactions:

$$2Mg+O_2 \rightarrow 2MgO$$

$$4B+3O_2 \rightarrow 2B_2O_3$$

[0102] The active content for B and Mg obtained from the TGA mass gain were calculated to be ~80% and ~88%, respectively.

[0103] Boron oxide (B_2O_3) was purchased from Alfa Aesar, and was ball milled to reduce the particle size to ~2 μm.

[0104] To reduce the particle size of B_2O_3 purchased from Alfa Aesar, a ball milling procedure was employed. Briefly, ~200 mg B_2O_3 and 1 mL hexane were added into a 2 mL centrifuge tube, followed by addition of 3 hardened steel and alumina balls (purchased from GlenMills, 7⁄32" in diameter). The tube was then loaded into a Retsch CryoMill operated at ambient conditions for milling (frequency of 25.0 Hz) for a total of 180 min with 18 cycles to avoid heat accumulation (one cycle was 10 min and interval between cycles was at least 5 min). More hexane was added during the process to maintain a roughly constant volume of hexane in the centrifuge tube. The milled samples were then collected and dried in vacuum oven at 150° C. for ~5 h. The average size of the particles was ~2 μm.

Preparation of Nanothermite Composites

[0105] The B—Mg/CuO nanothermite composites were prepared by adding the fuel and oxidizer components in hexane (10 mg/mL solid loading) followed by ~**1***h* of ultrasonication to achieve homogeneous particle mixing. The samples were then dried for 24 hours under ambient conditions to obtain the thermite powders. For these composites, incremental amounts of Mg particles were added while a constant B/CuO mass ratio was maintained to achieve a fuel:oxidizer equivalence ratio of 1 (B/CuO, ϕ=1). The composition of the formulations fabricated have been tabulated in Table 1.

TABLE 1

Different B/Mg-based mixtures fabricated with CuO oxidizer.

Mol % Mg	Wt. % Mg (total fuel, i.e., Mg + B)	Wt. % of B (total fuel, i.e., Mg + B)	Wt. % of Mg (total mixture, i.e., Mg + B + CuO)	Wt. % of B (total mixture, i.e., Mg + B + CuO)	Wt. % of CuO (total mixture, i.e., Mg + B + CuO)
0	0	100	0	9.6	90.4
3	6.5	93.5	0.7	9.6	89.7
6.6	13.4	86.6	1.5	9.5	89.1
10	19.9	80.1	2.3	9.4	88.3
15	28.4	71.6	3.7	9.3	87.1

[0106] Constant-volume combustion cell (~20 cm^{-3}) characterization was performed on 25.0 mg of the samples using the setup as described in Ghildiyal et al. *ACS Appl. Mater. Interfaces* 14(15) 17164-17174, 2022 and Ghildiyal et al. *ACS Appl. Mater. Interfaces* 13(1) 458-467, 2021.

Materials Characterization

[0107] Microscopic characterization of the samples was performed on an FEI NNS450 microscope operating at 18 kV. The nanoparticle structure and composition were characterized with an FEI Titan Themis **300** scanning transmission electron microscope (300 kV) with a high-angle annular dark-field detector (HAADF). Constant-volume combustion cell (~20 cm^3) measurements were performed on 25.0 mg of the fabricated thermite composites using a setup described in our previous studies. For thermogravimetric analysis and differential scanning calorimetry (TGA/DSC), a Netsch STA449 F3 Jupiter thermal analyzer was used. Ultrahigh purity argon (purity ~99.9999%) was used as the TGA atmosphere to prevent Mg particle oxidation. X-ray diffraction on the samples was performed with a PANanalytical Empyrean Series 2 diffractometer (Cu Ka radiation). Attenuated total reflection-Fourier transform infrared (ATR-FTIR) characterization on the samples was performed on a Nicolet iS50R spectrometer with a deuterated triglycine sulfate (DTGS) detector with a 4 cm^{-1} resolution. Crushed and dried KBr was used as a reference, and the spectra obtained were processed using Happ-Genzel apodization, Mertz phase correction, and atmospheric suppression.

T-Jump/TOFMS and Ignition Characterization

[0108] T-Jump/TOFMS and ignition temperature characterizations were performed to probe and investigate the reaction mechanisms in the fabricated composites at high heating rates (~10^5 K s^{-1}), as detailed in Ghildiyal et al. *ACS Appl. Mater. Interfaces* 13(1) 458-467, 2021 and Delisio et al. *J. Phys. Chem.* 120(24), 5534-5542, 2016. Briefly, a small quantity (~5 mg) of the prepared composites were dispersed in hexane and sonicated for ~10 min. The suspension was then drop cast on a platinum wire (~1 cm, 76 μm diameter) soldered to copper leads of the electrical feedthroughs. The samples were then heated with a ~3 ms pulse under a high vacuum (10° atm) to a maximum temperature of ~1400 K. Following thermal activation by the pulse, the gas-phase species evolved during the reaction were ionized with a 70-eV electron gun and probed with a multichannel plate detector for 10 ms with a temporal resolution of 100 μs. The ignition characterization of the samples was carried out with a high-speed camera (Vision Research Phantom v12.0) in an argon environment at 1 atm pressure. The ignition point was identified by correlating the optical emission obtain from the camera with the time and temperature obtained from wire heating.

Effect of Mg Addition on the Energetic Characteristics of B/CuO Composites

[0109] The effect of Mg NPs as an additive fuel on the reactivity and energy release of boron NP-based composites was explored. To evaluate this effect, B/Mg/CuO nanoenergetic composites were fabricated with varying additive content of Mg NPs, and their pressurization characteristics were characterized by constant-volume combustion cell measurements, as described in Ghildiyal et al. *ACS Appl. Mater. Interfaces* 14(15) 17164-17174, 2022. FIGS. **2**A, **2**B, **13**A and **13**B show the measured reactivity parameters (peak pressures, pressurization rates, and burn times) of B/Mg/CuO composites at different additive Mg loadings. Increasing Mg content resulted in enhanced reactivity of the composites with higher peak pressures and pressurization rates, and shorter burn times. Notably, Mg/B-based composites showed up to ~6-fold enhancement in pressurization rates and ~30% increase in peak pressures relative to B-based composites. Mg addition to B/CuO thermites shortened their burn time from ~6.5 ms to ~2 ms (~60% reduction), as shown in FIG. **2**B. The considerable reduction in the pressurization and burning timescales suggested that adding Mg to B-based composites augmented their reaction kinetics.

Mg-based composites (without B) fabricated with the highest additive Mg amount (15 mol %) did not ignite or show pressurization with CuO. This was expected, since from a compositional perspective, these composites would be highly fuel-lean since Mg was only a minor, additive fuel in these composites.

[0110] Based on these observations, the reactivity enhancement in Mg/B samples relative to Mg— or B-based composites suggested a synergistic effect between Mg and B fuels was likely responsible for the augmentation observed in FIGS. **2**A and **2**B, without wishing to be bound by the mechanism. The oxidation and energy release kinetics for boron are limited and greatly affected by the transport processes occurring through its oxide shell (B_2O_3). The reaction between Mg and the B_2O_3 shell of boron is exothermic and might be involved in the combustion of Mg/B-based composites. Notably, the exothermicity of the Mg/B_2O_3 reaction ($\Delta H \sim -550$ kJ mol^{-1}) is on par with that of the Mg/CuO ($\Delta H \sim -440$ kJ mol^{-1}) and B/CuO ($\Delta H \sim -600$ kJ mol^{-1}) systems both on a molar and gravimetric basis, as shown in Table 2.

[0111] The reaction mechanism of the Mg/B_2O_3 reaction was investigated to probe this reaction and its implications on reactivity enhancement of B NPs, as Mg/B_2O_3 was a simulant for the interaction of Mg with the oxide shell of boron (B_2O_3). Mg/B_2O_3 composites were fabricated assuming a stoichiometric redox reaction between the components ($\phi=1$) and their constant-volume pressurization and ignition characteristics were evaluated. As shown in FIG. **4**B, the Mg/B_2O_3 reaction initiation occurred at a relatively low temperature (ignition temperature) ~600° C. The Mg/B_2O_3 thermite system showed significant pressurization with a peak pressure of ~130 kPa and a pressurization rate of ~ 8 MPa/s. In comparison, B/CuO thermites showed ~65 kPa maximum pressure and ~10 MPa/s pressurization rate. The burn time of the Mg/B_2O_3 mixture (~14.2 ms) was on the same order of magnitude as that of the B/CuO samples (~6.5 ms, FIG. **2**B). Note that the B_2O_3 particles were much larger (~2 μm) than the B_2O_3 shell on B NPs, which may be on the order of tens of nm. Therefore, the reaction of Mg with the oxide shell was likely much faster than that for the simulant B_2O_3 particles. These results indicate that both Mg/B_2O_3 and B/CuO reactions could occur on a similar timescale, suggesting that Mg could potentially interact with the oxide shell (B_2O_3) of boron NPs in B/Mg-based composites s shown in FIGS. **2**A and **2**B.

Mg/B_2O_3 Reaction Mechanisms: Ignition, Thermal Analysis, and Reaction Product Characterization

[0112] The reactions and the associated thermochemistry potentially involved in the B/Mg/CuO thermite system are summarized in Table 2. The reaction of Mg with CuO and B_2O_3 are energetically comparable both on a gravimetric and a molar basis as seen in Table 2. FIGS. **14**A-**14**C show the ignition snapshots of B/CuO, Mg/CuO, and B/Mg(15%)/CuO mixtures in an argon atmosphere. The ignition temperatures of these mixtures, summarized in Table 2, showed a marginal decrease in the ignition temperature of B/Mg/CuO samples relative to B/CuO and Mg/CuO composites. The ignition temperature of the Mg/B_2O_3 reaction was significantly lower than that of B/CuO, Mg/CuO, and B/Mg/CuO mixtures (FIGS. **4**A, **4**B and **14**A-**14**C). Energetic reactions with Mg have been shown to be initiated by the release of Mg vapor. Therefore, the lower ignition temperature for Mg/B_2O_3 system (~600° C.) could be attributed to the molten B_2O_3 surface (melting point ~450° C.) acting as a favorable condensation site for Mg vapor to react with the oxidizer. On the other hand, the reaction of Mg vapor with CuO may be limited by the release of gas-phase O_2 following oxidizer decomposition at higher temperatures (~700° C.), resulting in significantly higher ignition thresholds (>700° C.).

[0113] Although the contribution from the Mg/CuO reaction cannot be completely neglected, it was noted that thermodynamically, Mg has relatively similar molar and gravimetric reaction enthalpies with both CuO and B_2O_3, as shown in Table 2. Moreover, the lower ignition temperature and early reaction onset for the Mg/B_2O_3 mixture than Mg/CuO and B/CuO thermites suggested that Mg could initiate the reaction with the oxide layer of B much earlier than its ignition and combustion with CuO. In the case of aluminum, pre-ignition reactions with its oxide shell (Al_2O_3) with reactive gases (e.g., HF, F_2) have been shown to significantly affect their combustion. Therefore, the low temperature, pre-ignition Mg/B_2O_3 surface reactions may play a significant role in surface disruption and reactivity enhancement of boron.

[0114] To further characterize the reaction between Mg and B_2O_3 thermogravimetric analysis/differential scanning calorimetry (TGA/DSC) and x-ray diffraction (XRD) analysis were performed on the Mg/B_2O_3 mixtures to further characterize the reaction between Mg and B_2O_3. FIG. **5**A shows the TGA/DSC curves for the Mg/B_2O_3 sample at a heating rate of 10° C./min. The TGA curve showed ~22% mass loss at ~100-200° C. with two endothermic peaks appearing in the DSC signal. The mass loss and the endotherms may be attributed to the multistep dehydration and decomposition of H_3BO_3 present in the B_2O_3 particles. More importantly, two distinct exotherms were observed occurring at ~500-650° C., indicating an exothermic redox reaction between Mg and B_2O_3. The reaction mixture was heated at different temperatures and the products were analyzed by XRD characterization. As shown in FIG. **5**B, the unheated mixture showed characteristic peaks for both Mg and B_2O_3. The peaks remained unchanged up to a temperature of ~500° C. However, when the samples were heated up to a temperature of ~500° C., the peaks for MgO began to appear, while the B_2O_3 and Mg peaks were highly diminished. At a higher temperature of ~650° C., no B_2O_3 and Mg peaks were observed, while MgO peaks were the most prominent (reaction approaching completion). At much higher temperatures (~1000° C.), peaks from ternary oxide, $Mg_3B_2O_6$, appeared, which likely formed because of an exothermic reaction between MgO and unreacted B_2O_3. These results suggested that the Mg/B_2O_3 reaction followed a two-step pathway— a magnesiothermic reduction of B_2O_3 particles to boron (~500-600° C.) followed by the reaction of MgO and unreacted B_2O_3 (>650° C.), as shown by the following reactions:

Step I: $3Mg+B_2O_3 \rightarrow 3MgO+B$

Step II: $3MgO+B_2O_3 \rightarrow Mg_3B_2O_6$

TABLE 2

Thermochemistry and ignition temperature measurements obtained for different possible reactive systems involved in B/Mg/CuO combustion. ΔH_{rm} and ΔH_{rg} represent the molar and gravimetric reaction enthalpy. Enthalpy values are calculated from the references mentioned.

Reactive system	Reaction	ΔH_{rm} (kJ g^{-1})	ΔH_{rg} (kJ g^{-1})	Ignition temperature (° C., +40° C.)
B/CuO	$2B + 3CuO \rightarrow B_2O_3 + 3Cu$ – (i)	−780	−3.0	760
Mg/CuO	$Mg + CuO \rightarrow MgO + Cu$ – (ii)	−440	−4.3	800
B/Mg/CuO	(i), (ii), (iii), (iv)	—	—	730
Mg/B_2O_3	$3Mg + B_2O_3 \rightarrow 3MgO + Cu$ – (iii)	−550	−3.9	600
MgO/B_2O_3	$3MgO + B_2O_3 \rightarrow Mg_3B_2O_6$	−110	−0.6	—

[0115] The Mg/B_2O_3 redox reaction was further corroborated by the absence of BOX (BO_3/BO_4), O—H, and B—O—B peaks in the FTIR spectra of the Mg/B_2O_3 mixtures heated at 650° C., as shown in FIG. **6**. These results were also consistent with the DSC data shown in FIG. **5**A, where exothermic peaks were observed between ~500-650° C. Moreover, the ignition temperature of the Mg/B_2O_3 mixture in argon also occurred around similar temperatures (**600**) ° C., as shown in FIG. **4**B. These observations confirmed that the Mg/B_2O_3 exothermic redox reaction occurred at relatively low temperatures ~500-650° C. Since these temperatures were higher than the melting point of B_2O_3 (~450° C.), it was postulated that the Mg likely reacts with B_2O_3 in a molten form.

Mg/B_2O_3 Reaction Mechanism: T-Jump/TOFMS and Implications on Oxide Shell Disruption of B NPs

[0116] To further probe the interaction between Mg and B_2O_3, the species evolved from thermally activated Mg/B_2O_3 reaction at a high heating rate (10^5 K/s) using T-jump/TOFMS were analyzed. FIG. **7**A shows the various species released from the Mg/B_2O_3 samples. The most prominent gas-phase species evolved from the sample were H_2O (m/z=18), Mg (m/z=24), and HOBO species (m/z=45, 62), as indicated in FIG. **7**A. A temporal profile of these species, shown in FIG. **7**B, revealed the mechanism of the Mg/B_2O_3 reaction. At low temperatures (~100-200° C.), desorption of adsorbed water and H_3BO_3 decomposition resulted in the release of H_2O and HOBO fragments (H_3BO_2 and H_3BO_3). At higher temperatures (~650° C.), the release of gas-phase Mg species was observed, as shown in FIG. **7**B. This result was consistent with a previous study, where rapid Mg vaporization and release of gas-phase Mg species were observed. Interestingly, the ignition of the Mg/B_2O_3 samples (FIG. **4**B) occurred following B_2O_3 melting and close to the release of vapor-phase Mg species, as demarcated in FIG. **7**B. These results suggested the exothermic reaction between Mg/B_2O_3 observed earlier (FIGS. **4**A-**6**) occurred by a heterogeneous reaction between vapor-phase Mg and molten B_2O_3, as illustrated later in FIG. **9**A. The Mg vapor-initiated heterogeneous reaction with the oxidizer surface (B_2O_3) was consistent with the reaction mechanism of Mg with the Bi_2O_3 oxidizer. In this case, the redox reaction and ignition were similarly controlled by the release of Mg vapor, which reacted with the Bi_2O_3 oxidizer surface and initiated ignition at the Mg vapor/oxidizer interface.

[0117] In order to investigate the effect of Mg directly on the B_2O_3 oxide layer of boron NPs, a mixture of Mg and B NPs (~10 mol % of Mg relative to total mixture) was prepared without any oxidizer, and DSC characterization was performed on the sample in ultrahigh purity argon. FIG. **8** shows the DSC curves of the Mg/B mixtures in argon compared to the Mg/B_2O_3 (Mg-boron oxide shell simulant mixture). Interestingly, two Mg/B reaction exotherms were observed around ~550-650° C., the range observed earlier for the reaction between B_2O_3 and Mg. This temperature was higher than the melting point of the oxide shell (B_2O_3, 450° C.) and close to the Mg vapor release temperature observed earlier (~650° C.). Therefore, the exotherms shown in the Mg/B DSC curve may be a result of the heterogeneous reaction of Mg vapor with the molten oxide shell of boron NPs, as shown in FIG. **9**B. In addition to the reaction with the B_2O_3 shell, the excess Mg may undergo further reaction with boron to form borides in the absence of an oxidizer.

[0118] The reaction mechanisms of the Mg/B_2O_3 system to Mg/B NP-based composites can be extrapolated, whereby Mg vapor reacts with the molten B_2O_3 shell, as illustrated in FIGS. **9**A and **9**B. The Mg/B_2O_3 reactions may have several physical implications on the structure of the oxide surface of boron, without wishing to be bound by the mechanisms. First, the Mg vapor-induced reduction of B_2O_3 to B creates a possibly pristine and accessible fuel surface for the reaction with the oxidizer. Secondly, further reaction of MgO with B_2O_3 to nucleate ternary oxides, as seen in the XRD, ($Mg_3B_2O_6$, FIG. **5**B) in the B_2O_3 liquid matrix may result in oxide shell thinning due to the wetting effects from the liquid around the solid oxide particles. Similar particle wetting effects have been observed in B/Bi_2O_3 thermites and have been proposed to result in facilitated ignition. These effects may enhance the combustion of boron by increasing the accessible reactive fuel surface to the oxidizer. These effects were supported by the overlapping Mg, B, and O domains observed in the SEM-EDS images of the combustion products of B/Mg/CuO composites (FIGS. **15** and **16**).

[0119] The XRD patterns of the powders, shown in FIGS. **15** and **16**, revealed peaks primarily from Cu as one of the products of the redox reaction between fuel and oxidizer components. The peaks from either MgO, B_2O_3, or $Mg_3B_2O_3$ were missing, suggesting that these products were likely amorphous or absent. The SEM-EDS maps of the combustion product of B/Mg(15%)/CuO showed relatively large particulates composed of Cu and Mg/B oxide. Due to the poor signal quality from B (low X-ray energy) in SEM-EDS, drawing definitive conclusions was challenging. Qualitatively, Mg, B, and O overlapping domains were observed as indicated in FIGS. **15**/**16**, suggesting possible synergistic interactions between Mg and B fuels during combustion.

[0120] Lastly, the exothermic reactions may also increase the local temperature of the unreacted B_2O_3 shell, and assist in its physical vaporization and removal, thereby contributing to the reaction rate enhancement of boron particle oxidation. Prior studies have observed that reactive gas-phase species that can react with the B_2O_3 shell may assist in its removal and lead to enhanced boron combustion. Assuming a 50% reaction between Mg and B_2O_3 shell, and

further assuming the exothermicity of the reaction is localized on the oxide shell (neglecting all heat losses), a simple energy balance yields an extremely high local surface temperature (T ~3200° C. >boiling point of B_2O_3 ~1860).

[0121] The surface temperature of the oxide layer of B NPs due to its reaction with Mg vapor was estimated according to the following redox reaction:

$$3Mg+B_2O_3 \rightarrow 3MgO+B \quad \Delta H_r=-420 \text{ kJ/mol}$$

[0122] Assuming 50 mol % of the B_2O_3 was consumed by the Mg and the heat released was localized on the remnant oxide shell of boron particles, the local temperature increase could be estimated according to the following equation:

$$\Delta T_{ox} = \frac{\Delta H_{ox}}{m_{ox.} C_{p,ox}}$$

[0123] where ΔT_{ox} was the temperature rise of the remaining B_2O_3 layer, ΔH, was the heat generated from the reaction of 50 mol % of B_2O_3 with Mg (ΔH_{ox}=1.3×10-17 J), m_{ox}. was the mass of the oxide layer (=3.6×10^{-18} kg, thickness ~5 nm), $C_{p,\ ox}$ was the specific heat capacity of the oxide layer (=129.6 J mol^{-1}° $C.^{-1}$).

[0124] Using these values, the estimated temperature increase of the B_2O_3 layer was ~3200° C. Note that these values were obtained without considering any heat losses in the system.

[0125] Of course, the actual temperature of the shell may be considerably lower than this value due to the heat losses involved. Nevertheless, the estimates and the observations above suggested that the Mg/B_2O_3 (oxide shell) reaction system possessed sufficient energy required for the vaporization of the molten B_2O_3 layer. These results indicated that additional surface reactions relating to the interaction of Mg with the oxide shell of boron particles contributed significantly to their reactivity enhancement.

Example 2: Magnesium-Induced Surface Disruption of Silicon, Titanium, and Aluminum Oxide Surfaces

[0126] Nanoscale reactive metals and metalloids such as Al, Ti, and Si are attractive commercially available fuels for nanoenergetic composites due to their high energy densities. However, the inert native oxide shells on the surfaces of these fuels (Al_2O_3, TiO_2, and SiO_2) present kinetic diffusional barriers to reactive species, hindering their oxidation and energy. The inert oxide layer adds dead mass to the energetic mixture and reduces their overall energy content. Nanoscale Mg has been shown to undergo rapid vaporization, releasing highly reactive Mg vapor which can corrode the surface of boron nanoenergetic composites by reacting exothermically with its B_2O_3 layer, resulting in enhanced burn characteristics. Since Mg also shows similar exothermic redox reactions with Al_2O_3, TiO_2, and SiO_2 (as shown in Table 3), adding Mg to other nanoscale fuels (nAl/nTi/nSi) may show a similar enhancement in their energy release and total by reacting with their oxide shell.

[0127] Mg NPs were prepared as described in Example 1. Unless specified otherwise, experiments were performed similarly to those described in Example 1. The active content of the fuels (Ti, Al, Si, and Mg) were estimated from the mass gain upon oxidation in air or O_2. Nanopowers of titanium oxide (TiO_2), silicon oxide (SiO_2), and aluminum oxide (Al_2O_3) were purchased from commercially available sources, and were used as received.

TABLE 3

Thermochemistry of the exothermic heterogeneous reactions of Mg vapor with metal oxide surfaces.

Oxide layer	Reaction with Mg	ΔH (KJ/mol)	ΔH (J/g)
Al_2O_3	$3Mg + Al_2O_3 \rightarrow 3MgO + 2Al$	−130	−740
TiO_2	$2Mg + TiO_2 \rightarrow 2MgO + Ti$	−260	−2060
SiO_2	$2Mg + SiO_2 \rightarrow 2MgO + Si$	−290	−2690

[0128] As shown in FIGS. **17**A and **17**B, Mg NPs showed violent reactions and ignition with nanoscale SiO_2 and TiO_2, both of which can be considered as simulant materials for the oxide surfaces of Ti and Si. This suggested that the reaction of Mg with the oxide shells of these fuels is feasible at high heating rates and can potentially improve their combustion characteristics. The XRD patterns of products obtained by heating Mg with Al_2O_3 and SiO_2 at 500° C. are shown in FIGS. **18**A and **18**B. As evidenced by the appearance of zero-valent Si and Al peaks along with the signals from alloy products (Mg_2Al_3, Mg_2Si), it was determined that Mg NPs can undergo exothermic redox and alloying reactions with the oxide surface materials of Al and Si fuels. The reactions showed promise in enhancing the reactivity of these fuels by local heat generation and surface etching of their oxide shells.

Example 3: Mg—Ti/CuO Compositions

Preparation of Nanothermite Composites

[0129] The Mg—Ti/CuO nanothermite composites were prepared by adding the fuel and oxidizer components in hexane (10 mg/mL solid loading) followed by ~**1***h* of ultrasonication to achieve homogeneous particle mixing. The samples were then dried for 24 hours under ambient conditions to obtain the thermite powders. For these composites, incremental amounts of Mg particles were added while a constant Ti/CuO mass ratio was maintained to achieve a fuel:oxidizer equivalence ratio of 1 (Ti/CuO, ϕ=1). Constant-volume combustion cell (~20 cm^{-3}) characterization was performed on 25.0 mg of the samples using the setup described in prior works.

[0130] Unless specified otherwise, experiments were performed similarly to those described in Example 1. Preliminary results with additive amounts of Mg to Ti/CuO mixtures showed an enhancement in pressurization and burn characteristics, as shown in FIGS. **19**A and **19**B. The pressurization rate showed ~5-fold enhancement, while the burn time was reduced by ~52%. This result indicated that the addition of small additive quantities of Mg to Ti significantly promoted its combustion, similar to the effect observed in B/CuO composites.

[0131] While this specification contains many specifics, these should not be construed as limitations on the scope of an invention or of what may be claimed, but rather as descriptions of features specific to particular embodiments of the invention. Certain features that are described in this specification in the context of separate embodiments can

also be implemented in combination in a single embodiment. Conversely, various features that are described in the context of a single embodiment can also be implemented in multiple embodiments separately or in any suitable subcombination. Moreover, although features may be described above as acting in certain combinations and even initially claimed as such, one or more features from a claimed combination can in some cases be excised from the combination, and the claimed combination may be directed to a subcombination or a variation of a subcombination.

[0132] Only a few implementations are disclosed. However, variations and enhancements of the disclosed implementations and other implementations can be made based on what is described and illustrated in this specification.

[0133] References listed below and included herein are incorporated by reference in their entirety.

[0134] (1) Jiang, Y.; Deng, S.; Hong, S.; Zhao, J.; Huang, S.; Wu, C.-C.; L. Gottfried, J.; Nomura, K.; Li, Y.; Tiwari, S.; et al. Energetic Performance of Optically Activated Aluminum/Graphene Oxide Composites. *ACS Nano* 2018, 12 (11), 11366-11375. https://doi.org/10.1021/acsnano.8b06217.

[0135] (2) Dreizin, E. L. Metal-Based Reactive Nanomaterials. *Progress in Energy and Combustion Science*. Pergamon Apr. 1, 2009, pp 141-167. https://doi.org/10.1016/j.pecs.2008.09.001.

[0136] (3) Rehwoldt, M. C.; Yang, Y.; Wang, H.; Holdren, S.; Zachariah, M. R. Ignition of Nanoscale Titanium/Potassium Perchlorate Pyrotechnic Powder: Reaction Mechanism Study. *J. Phys. Chem*. C 2018, 122 (20), 10792-10800. https://doi.org/10.1021/acs.jpcc.8b03164.

[0137] (4) Wang, J.; Zhang, L.; Shen, J.; Li, Z. Highly Reactive PTFE/Mg Nanolaminates and Its Combustion Performances. *Adv. Mater. Interfaces* 2019, 6 (14). https://doi.org/10.1002/ADMI.201900113.

[0138] (5) Valluri, S. K.; Schoenitz, M.; Dreizin, E. Bismuth Fluoride-Coated Boron Powders as Enhanced Fuels. *Combust. Flame* 2020, 221, 1-10. https://doi.org/10.1016/J.COMBUSTFLAME.2020.07.023.

[0139] (6) Chintersingh, K. L.; Sun, Y.; Schoenitz, M.; Dreizin, E. L. Heterogeneous Reaction Kinetics for Oxidation and Combustion of Boron. *Thermochim. Acta* 2019, 682, 178415. https://doi.org/10.1016/J.TCA.2019.178415.

[0140] (7) Yeh, C. L.; Kuo, K. K. Ignition and Combustion of Boron Particles. *Prog. Energy Combust. Sci.* 1996, 22 (6), 511-541. https://doi.org/10.1016/S0360-1285(96)00012-3.

[0141] (8) Mursalat, M.; Schoenitz, M.; Dreizin, E. L. Effect of Particle Morphology on Reactivity, Ignition and Combustion of Boron Powders. *Fuel* 2022, 324. https://doi.org/10.1016/j.fuel.2022.124538.

[0142] (9) Jain, A.; Joseph, K.; Anthonysamy, S.; Gupta, G. S. Kinetics of Oxidation of Boron Powder. *Thermochim. Acta* 2011, 514 (1-2), 67-73. https://doi.org/10.1016/J.TCA.2010.12.004.

[0143] (10) Chintersingh, K. L.; Schoenitz, M.; Dreizin, E. L. Oxidation Kinetics and Combustion of Boron Particles with Modified Surface. *Combust. Flame* 2016, 173, 288-295. https://doi.org/10.1016/J.COMBUSTFLAME.2016.08.027.

[0144] (11) Baek, J.; Jiang, Y.; Demko, A. R.; Jimenez-Thomas, A. R.; Vallez, L.; Ka, D.; Xia, Y.; Zheng, X. Effect of Fluoroalkylsilane Surface Functionalization on Boron Combustion. *ACS Appl. Mater. Interfaces* 2022. https://doi.org/10.1021/ACSAMI.2C00347/SUPPL_FILE/AM2C00347_SI_005. AVI.

[0145] (12) Wang, J.; Mao, Y.; Chen, J.; Li, Z. J.; Wang, J.; Nie, F. Surface Engineering Boron/Graphite Fluoride Composite with Enhanced Ignition and Combustion Performances. Fuel 2022, 323, 124374. https://doi.org/10.1016/J.FUEL.2022.124374.

[0146] (13) Valluri, S. K.; Schoenitz, M.; Dreizin, E. Boron-Metal Fluoride Reactive Composites: Preparation and Reactions Leading to Their Ignition. *J. Propuls. Power* 2019, 35 (4), 802-810. https://doi.org/10.2514/1.B37306.

[0147] (14) Abraham, A.; Obamedo, J.; Schoenitz, M.; Dreizin, E. L. Effect of Composition on Properties of Reactive Al.B.12 Powders Prepared by Mechanical Milling. *J. Phys. Chem. Solids* 2015, 83, 1-7. https://doi.org/10.1016/j.jpcs.2015.03.005.

[0148] (15) Zhang, B.; Huang, C.; Yan, S.; Li, Y.; Cheng, Y. Enhanced Reactivity of Boron, through Adding Nano-Aluminum and Wet Ball Milling. *Appl. Surf. Sci.* 2013, 286, 91-98. https://doi.org/10.1016/J.APSUSC.2013.09.026.

[0149] (16) Liu, J. Z.; Xi, J. F.; Yang, W. J.; Hu, Y. R.; Zhang, Y. W.; Wang, Y.; Zhou, J. H. Effect of Magnesium on the Burning Characteristics of Boron Particles. *Acta Astronaut.* 2014, 96 (1), 89-96. https://doi.org/10.1016/J.ACTAASTRO.2013.11.039.

[0150] (17) Hashim, S. A.; Karmakar, S.; Roy, A. Effects of Ti and Mg Particles on Combustion Characteristics of Boron-HTPB-Based Solid Fuels for Hybrid Gas Generator in Ducted Rocket Applications. *Acta Astronaut.* 2019, 160, 125-137. https://doi.org/10.1016/J.ACTAASTRO.2019.04.002.

[0151] (18) Xu, F.; Biswas, P.; Nava, G.; Schwan, J.; Kline, D. J.; Rehwoldt, M. C.; Mangolini, L.; Zachariah, M. R. Tuning the Reactivity and Energy Release Rate of 1205 Based Ternary Thermite Systems. *Combust. Flame* 2021, 228, 210-217. https://doi.org/10.1016/J.COMBUSTFLAME.2020.12.047.

[0152] (19) Zhao, W.; Wang, X.; Wang, H.; Wu, T.; Kline, D. J.; Rehwoldt, M.; Ren, H.; Zachariah, M. R. Titanium Enhanced Ignition and Combustion of Al/1205 Mesoparticle Composites. *Combust. Flame* 2020, 212, 245-251. https://doi.org/10.1016/j.combustflame.2019.04.049.

[0153] (20) Ghildiyal, P.; Biswas, P.; Herrera, S.; Xu, F.; Alibay, Z.; Wang, Y.; Wang, H.; Abbaschian, R.; Zachariah, M. R. Vaporization-Controlled Energy Release Mechanisms Underlying the Exceptional Reactivity of Magnesium Nanoparticles. *ACS Appl. Mater. Interfaces* 2022, 14 (15), 17164-17174. https://doi.org/10.1021/ACSAMI.1C22685/ASSET/IMAGES/MEDIUM/AM1C22685_M 002.GIF.

[0154] (21) Liu, X.; Chintersingh, K. L.; Schoenitz, M.; Dreizin, E. L. Reactive Composite Boron-Magnesium Powders Prepared by Mechanical Milling. *J. Propuls. Power* 2018, 34 (3), 787-794. https://doi.org/10.2514/1.B36315.

[0155] (22) Ghildiyal, P.; Ke, X.; Biswas, P.; Nava, G.; Schwan, J.; Xu, F.; Kline, D. J.; Wang, H.; Mangolini, L.; Zachariah, M. R. Silicon Nanoparticles for the Reactivity and Energetic Density Enhancement of Energetic-Bio-

cidal Mesoparticle Composites. *ACS Appl. Mater. Interfaces* 2021, 13 (1), 458-467. https://doi.org/10.1021/acsami.0c17159.

[0156] (23) Delisio, J. B.; Hu, X.; Wu, T.; Egan, G. C.; Young, G.; Zachariah, M. R. Probing the Reaction Mechanism of Aluminum/Poly(Vinylidene Fluoride) Composites. *J. Phys. Chem.* B 2016, 120 (24), 5534-5542. https://doi.org/10.1021/acs.jpcb.6b01100.

[0157] (24) Keerthi, V.; Nie, H.; Pisharath, S.; Hng, H. H. Combustion Characteristics of Fluoropolymer Coated Boron Powders. *Combust. Sci. Technol.* 2020, 194 (6), 1183-1198. https://doi.org/10.1080/00102202.2020.1804885.

[0158] (25) Wang, S.; Liu, X.; Schoenitz, M.; Dreizin, E. L. Nanocomposite Thermites with Calcium Iodate Oxidizer. *Propellants, Explos. Pyrotech.* 2017, 42 (3), 284-292. https://doi.org/10.1002/prep.201600213.

[0159] (26) Xi, J.; Liu, J.; Wang, Y.; Liang, D.; Li, H.; Zhou, J. Role of Oxalic Acid in Promoting Ignition and Combustion of Boron: An Experimental and Theoretical Study. *Propellants, Explos. Pyrotech.* 2014, 39 (6), 844-851. https://doi.org/10.1002/PREP.201400048.

[0160] (27) NIST Chemistry WebBook, SRD 69 https://webbook.nist.gov.

[0161] (28) Materials Project.

[0162] (29) Li, Y.; Li, J.; Wang, B.; Ma, H.; Han, Z. An Approach to the Induced Reaction Mechanism of the Combustion of the Nano-Al/PVDF Composite Particles. *Surf. Coatings Technol.* 2022, 429, 127912. https://doi.org/10.1016/J.SURFCOAT.2021.127912.

[0163] (30) Huber, C.; Jahromy, S. S.; Birkelbach, F.; Weber, J.; Jordan, C.; Schreiner, M.; Harasek, M.; Winter, F. The Multistep Decomposition of Boric Acid. *Energy Sci. Eng.* 2020, 8 (5), 1650-1666. https://doi.org/10.1002/ESE3.622.

[0164] (31) Wang, X.; Wu, T.; Wang, H.; DeLisio, J. B.; Yang, Y.; Zachariah, M. R. Boron Ignition and Combustion with Doped 8-Bi203: Bond Energy/Oxygen Vacancy Relationships. *Combust. Flame* 2018, 197, 127-133. https://doi.org/10.1016/J.COMBUSTFLAME.2018.07.015.

We claim:

1. A composition, comprising:

magnesium nanoparticles;

a nanoscale metal or metalloid selected from the group consisting of boron, silicon, titanium, and aluminum; and

an oxidizer,

wherein the composition has a burn time reduced by about 50% to about 60% when compared to a second composition comprising the same amount of the oxidizer and the nanoscale metal or metalloid but without the magnesium nanoparticles.

2. The composition of claim **1**, wherein the oxidizer comprises the first oxide of the metal or metalloid.

3. The composition of claim **2**, wherein the first oxide of the metal or metalloid is a native oxide shell of the metal or metalloid.

4. The composition of claim **1**, wherein the oxidizer comprises one or more second oxides selected from the group consisting of CuO, B_2O_3, Al_2O_3, TiO_2, and SiO_2.

5. The composition of claim **1**, wherein the nanoscale metal or metalloid has an average particle size of about 390 nm to about 420 nm.

6. The composition of claim **1**, wherein the magnesium nanoparticles have an average particle size of about 350 nm to about 400 nm.

7. The composition of claim **1**, wherein the molar of the magnesium nanoparticles over the total molar of the magnesium nanoparticles and the nanoscale metal or metalloid is about 3.0% to about 15.0%.

8. The composition of claim **1**, wherein the molar ratio of the nanoscale metal or metalloid over the oxidizer is about +/−20% of the stoichiometric ratio.

9. The composition of claim **4**, wherein the molar ratio of the nanoscale metal or metalloid over the total molar of the one or more second oxides is about +/−20% of the stoichiometric ratio.

10. The composition of claim **1**, wherein the molar ratio of the oxidizer over the nanoscale metal or metalloid is about +/−20% of the stoichiometric ratio.

11. The composition of claim **4**, wherein the molar ratio of the total molar of the one or more second oxides over the nanoscale metal or metalloid id about +/−20% of the stoichiometric ratio.

12. The composition of claim **1**, wherein the weight percent of the nanoscale metal or metalloid of the total weight of the composition is about 9.0% to about 10.5%.

13. The composition of claim **1**, wherein the weight percent of the magnesium nanoparticles of the total weight of the composition is about 0.5% to about 4.0%.

14. The composition of claim **1**, wherein the peak pressure of the composition is increased by about 15% to about 30% over the peak pressure of the second composition.

15. The composition of claim **1**, wherein the pressurization rate of the composition is increased by about 5-fold to about 6-fold over the pressurization rate of the second composition.

16. The composition of claim **1**, wherein the composition has a burn time reduced by about 4.0 ms to about 5.0 ms over the burn time of the second composition.

17. The composition of claim **1**, wherein the composition has an ignition temperature lower than the ignition temperature of the second composition.

18. The composition of claim **1**, wherein the composition has an ignition temperature of about 500° C. to about 750° C.

19. A method of fabricating the composition of claim **1**, the method comprising:

dispersing the magnesium nanoparticles, the nanoscale metal or metalloid; and

drying the first composition to provide the composition of claim **1**.

20. The method of claim **19**, wherein the first solvent is an organic solvent that does not contain oxygen, or a mixture of multiple organic solvents that do not contain oxygen.

* * * * *